

A novel alveolar Krebs cycle-triggered CO₂ sensing mechanism regulates regional pulmonary ventilation.

Sascha Tank, Marc-Oliver Tritt, Kai Heckel, Paula Keller, Martina Kiefmann, Leonie Schulte-Uentrop, Alwin E. Goetz, Rainer Kiefmann

Department of Anesthesiology, University Hospital Hamburg-Eppendorf, Martinistrasse 52,
20251 Hamburg, Germany

Corresponding author:

Rainer Kiefmann, MD PhD

University Hospital Hamburg-Eppendorf

Department of Anesthesiology

Martinistrasse 52

20251 Hamburg, Germany

phone: (49) 40 7410-57632

fax: (49) 40 7410-57631

e-mail: r.kiefmann@uke.de

Abstract

Pulmonary perfusion disorders provoke atelectasis in order to minimize ventilation/perfusion mismatch. However, the underlying mechanisms remain unknown. Because intraalveolar CO₂ concentration ([CO₂]_{iA}) declines as a consequence of poor pulmonary perfusion we postulated the existence a novel alveolar CO₂-sensing mechanism which adapts the ventilation to perfusion. Real-time fluorescence imaging of rat lungs revealed that low [CO₂]_{iA} decreased cytosolic and increased mitochondrial Ca²⁺ in alveolar epithelial cells (AEC), leading to reduction of surfactant secretion and alveolar ventilation. Mitochondrial inhibition by ruthenium red or rotenone blocked the hypocapnia-induced responses. In cultured Type 2 AEC hypocapnia decreased cytosolic Ca²⁺ independently from pH and increased the NADH production, the mitochondrial transmembrane potential ($\Delta\Psi$), and subsequently the mitochondrial Ca²⁺ uptake. All responses were completely blocked by the gene knockdown of the NADH producing Krebs cycle enzyme isocitrate dehydrogenase. Furthermore, ligation of the pulmonary artery of rabbits decreased alveolar ventilation, surfactant secretion, and lung compliance. Addition of 5% CO₂ to the inspiratory gas inhibited all responses. Accordingly, we provide evidence for a novel CO₂-sensing mechanism of AEC regulated by the Krebs cycle activity in terms of a negative feedback loop adapting surfactant secretion and thus regional ventilation to pulmonary perfusion.

Keywords: alveolar carbon dioxide sensing, calcium, surfactant secretion, mitochondria, regional ventilation

Introduction

The mismatch between alveolar ventilation and perfusion is a typical complication in critically ill patients and results in gas exchange failure and reduction of oxygen delivery to systemic circulation.

Ventilation disorders, as seen in pneumonia or atelectasis, are associated with regional alveolar hypoxia which evokes vasoconstriction of the pulmonary arteries. This well known response is termed hypoxic pulmonary vasoconstriction (HPV) and shifts as a compensatory mechanism blood from poorly to better ventilated lung segments, thereby reducing shunt fraction and optimizing gas exchange.

Perfusion disorders occurring during pulmonary artery embolism or systemic inflammation with intravascular coagulation cause a reduction of ventilation in poorly perfused lung segments. This response seems to be a mechanism that opposes HPV and was first described in 1934 by Moore, Humphreys and Cochrane. They showed that in dogs an occlusion of the left pulmonary artery leads to a ventilation reduction of the ipsilateral lung with simultaneously ventilation increase in the contralateral lung¹. Occluding the right pulmonary artery induced a ventilation shift from right to left lung. Venrath *et al.* were able to demonstrate in 1952 the same ventilation shift in dogs using bronchspirometry². Swenson and co-workers published similar results in 1961 after pulmonary artery occlusion in patients using a balloon catheter³.

Although the perfusion-mediated regulation of ventilation has been described by several authors, the underlying mechanism has never been elucidated.

Ventilation, at least in part, is regulated by surfactant which is secreted from Type 2 cells by exocytosis of lamellar bodies (LB). Secreted surfactant promotes alveolar opening by opposing the alveolar-collapsing tendency of air-liquid surface tension. LB exocytosis is triggered by an increase of cytosolic Ca^{2+} concentration ($[\text{Ca}^{2+}]_{\text{cyt}}$) in Type 2 cells, which results from direct effects of agonists or cell stretch⁴⁻⁶.

We considered that alveolar CO_2 may play a crucial role in this scenario. Assuming that alveolar CO_2 concentration drops in non-perfused but still ventilated alveoli the alveolar CO_2 concentration could signal whether the alveolus is being perfused. We therefore hypothesized that, in case of perfusion disorder, the decline of alveolar CO_2 concentration initiates a reduction of ventilation by regulating LB exocytosis in order to normalize the ventilation-perfusion ratio.

CO_2 measurement systems have been described for plants and questionably for the brain stem^{7,8}. However, a CO_2 -sensing mechanism of alveolar epithelial cells in order to regulate the LB exocytosis and thus ventilation to changes in perfusion by a Ca^{2+} -signal transduction pathway is still unknown.

In this context, the mitochondria require consideration. Mitochondria regulate $[\text{Ca}^{2+}]_{\text{cyt}}$ by sequestering Ca^{2+} and releasing it to the cytosol⁹⁻¹⁴. The mitochondrial accumulation of Ca^{2+} is facilitated by the Ca^{2+} uniporter which is located in the inner mitochondrial membrane¹³. Ca^{2+} is stored inside the mitochondrial matrix in the form of osmotically inactive precipitates or is released back to the cytosol through the $\text{Ca}^{2+}/\text{Na}^+$ or $\text{Ca}^{2+}/\text{H}^+$ exchanger, which are also located on the inner membrane of the mitochondria¹³. The driving force for mitochondrial Ca^{2+} uptake is the negative transmembrane potential gradient ($\Delta\Psi$) across the mitochondrial inner membrane¹⁴. The membrane potential is component of the proton-motive gradient and

is set up through proton extrusion by the respiratory chain. Regulation of the respiratory chain activity and thus $\Delta\Psi$ is complex. However, there are some indications that the rate of respiration can be stimulated by NADH. This respiratory chain substrate is produced in the Krebs cycle by the enzymes isocitrate dehydrogenase and α -ketoglutarate dehydrogenase¹⁵⁻¹⁷ together with CO₂.

It is a common effect that an accumulation of the product may inhibit whereas a rapid clearance of the product may accelerate its enzymatic reaction rate. We therefore hypothesize that a pulmonary perfusion failure induces a decrease of [CO₂]_{iA} which in turn increases the production of NADH and thus $\Delta\Psi$ in AEC inducing a Ca²⁺-shift from the cytosol to the mitochondria. Furthermore, Kafta *et al.* have demonstrated that a Ca²⁺ shift into mitochondria abrogates increases of [Ca²⁺]_{cyt} and subsequently diminishes Ca²⁺-dependent membrane exocytosis¹⁸. However, the role of the Krebs cycle in CO₂-sensing and surfactant secretion has not been described so far.

Using fluorescence microscopy of the lung that enables *in situ* live imaging of intact alveoli we could describe for the first time that alveolar epithelial cells response to changes of [CO₂]_{iA} with a cytosolic Ca²⁺-signaling. In case of alveolar hypocapnia, as seen during pulmonary perfusion failure, Ca²⁺ is shifted from the cytosol to the mitochondria regulated by an increase of the Krebs cycle activity. In turn, surfactant secretion and alveolar ventilation is reduced in order to minimize ventilation/perfusion mismatch. Furthermore, using *in vivo* imaging of lung surface and a pulmonary artery ligation model we could demonstrate that CO₂ admixed to the inspiratory gas inhibits the reduction of ventilation in non-perfused lung areas.

Results

CO₂ regulates cytosolic calcium concentration [Ca²⁺]_{cyt} in alveolar epithelial cells *in situ*.

By means of alveolar micropuncture, we loaded alveolar epithelial cells with the Ca²⁺ fluorophore fura 2. The fura 2-loaded alveolus imaged as a circular fluorescent band that circumscribed a central nonfluorescent lumen. After establishing of alveolar hypocapnic conditions with an inspiratory CO₂ fraction of 0% and with lung venous pCO₂ of under 10 mmHg, [Ca²⁺]_{cyt} decreased in alveolar epithelial cells by 40±5 nM (mean±SE, p<0.05) versus baseline conditions within 10 minutes. This decrease was reversible after increasing the inspiratory CO₂ fraction back to 5% and the pCO₂ to normocapnic values. Hypercapnic alveolar conditions with an inspiratory CO₂ fraction of 10% and pCO₂ of 80 mmHg increased [Ca²⁺]_{cyt} in alveolar epithelial cells by 45±3 nM (mean±SE, p<0.05). This increase was also reversible after lowering the inspiratory CO₂ fraction and the pCO₂ to normocapnic values (figure 1A-C).

CO₂ sensing is mitochondrial triggered *in situ*. To determine the role of mitochondria in the CO₂-mediated calcium signaling we microinjected into the alveolus ruthenium red, an inhibitor of the mitochondrial Ca²⁺ uniporter, or rotenone, an inhibitor of the complex I of the respiratory chain. Pretreatment with ruthenium red inhibited the hypocapnia-induced decrease of [Ca²⁺]_{cyt} by about 50%. Rotenone blocked the hypocapnia-induced calcium decrease completely (figure 1D). Under normocapnic conditions neither ruthenium red nor rotenone did affect fura 2 ratio.

Furthermore, we microinjected into the alveolus rhod 2, a fluorescent dye for mitochondrial Ca²⁺ measurement, in combination with MTG for mitochondrial co-localisation (figure 2A). Hypocapnia induced an increase of rhod 2 fluorescence intensity equivalent for a rise of [Ca²⁺]_{mito} (figure 2B). Taken together, these results indicate that the hypocapnia-induced decrease of [Ca²⁺]_{cyt} was evoked by a calcium shift from the cytosol to the mitochondria mediated by the mitochondrial Ca²⁺ uniporter and complex I.

Hypocapnia-dependent regulation of [Ca²⁺]_{cyt} is pH-independent *in vitro*. In A549 cells the [Ca²⁺]_{cyt} responses to hypo- or hypercapnia were equivalent to those in the isolated lung (figure 3A,B). To test whether the [Ca²⁺]_{cyt} changes were induced rather by pH than CO₂ we measured in A549 cells the effect of CO₂ on [Ca²⁺]_{cyt} at a constant pH of 7.4. We could demonstrate that hypocapnia induced under constant extracellular pH of 7.4 similar reduction of [Ca²⁺]_{cyt} as in unbuffered cells at a pH of 7.8 (figure 3B). In contrast, an alkalosis of 7.8 under normocapnic conditions did not induce an alteration of [Ca²⁺]_{cyt}. Furthermore, in unbuffered cells hypocapnia did not alter the cytosolic pH (figure 3D). We therefore conclude that the hypocapnia-induced [Ca²⁺]_{cyt} responses were pH independent.

Hypocapnia-induced cytosolic Ca²⁺ shift is mitochondrial ΔΨ-mediated *in vitro*.

Suspecting that hypocapnia induces a Ca²⁺ shift from cytosol into mitochondria through an alteration of the mitochondrial membrane potential we loaded A549 cells with TMRM. Induction of hypocapnia at constant pH of 7.4 led to an increase of the ratio between the mitochondrial and cytosolic TMRM fluorescence intensity equivalent for increase of the mitochondrial ΔΨ (figure 4A,B). This response was blocked by rotenone (figure 4C,D). Since rotenone also inhibited the hypocapnia-induced decrease of [Ca²⁺]_{cyt} (figure 1D), we conclude that hypocapnia induces a Ca²⁺ shift from cytosol into the mitochondrium through an increase of the mitochondrial membrane potential.

Hypocapnia-induced increase of the mitochondrial ΔΨ and thus decrease of [Ca²⁺]_{cyt} is NADH-mediated *in vitro*. The Krebs cycle enzyme isocitrate dehydrogenase (IDH) catalyzes

oxidative decarboxylation of isocitrate to α -ketoglutarate and requires NAD^+ , producing NADH. In turn, NADH is utilised in the respiratory chain which is necessary to sustain the mitochondrial membrane potential. To elucidate whether hypocapnia induces an acceleration of the NADH production which in turn increases $\Delta\Psi$ and subsequently provokes a Ca^{2+} shift from the cytosol to the mitochondria we downregulated the NADH producing IDH3G (figure 4E). The decrease of $[\text{Ca}^{2+}]_{\text{cyt}}$ and the increase of $[\text{Ca}^{2+}]_{\text{mito}}$ or $\Delta\Psi$ following hypocapnia at constant pH of 7.4 was detectable in native and scrambled siRNA-treated A549 cells (figure 4F-H,A,B). However, all responses were completely absent in IDH3G downregulated cells (figure 4F-H,A,B). Additionally, in native cells hypocapnia increases the NADH-concentration in comparison to normocapnia measured by the biochemical NADH assay (figure 4I). This increase was elevated after inhibition of the NADH consuming complex 1 with rotenone (figure 4I). Furthermore, in control and scrambled siRNA-treated cells NADH autofluorescence increased following rotenone, which blocks the NADH consuming mitochondrial complex 1 (figure 4J,K). This increase was elevated upon induction of hypocapnia (figure 4J,K). In contrast, NADH fluorescence stayed stable following IDH3G gene knockdown (figure 4J,K). Taken together we conclude that under hypocapnic conditions Krebs cycle activity, NADH production, and thus $\Delta\Psi$ increase and subsequently $[\text{Ca}^{2+}]_{\text{cyt}}$ decreases independently from pH.

CO_2 -mediated mitochondrial Ca^{2+} shift regulates surfactant secretion *in situ*. Figure 5A shows images of alveolar epithelial type II cells (AEC Type 2) after alveolar loading with LTG, a specific fluorescent dye for surfactant in the surfactant-storing lamellar bodies. Under normocapnic conditions LTG-intensity linearly decreased indicating a constant level of surfactant secretion. Hypocapnia induced an inhibition of the LTG fluorescence decrease indicating a reduction of surfactant secretion, whereas hypercapnia accelerates the decrease of the LTG fluorescence intensity and thus surfactant secretion *in situ* (figure 5B and C) within 20 min. Hence, the rate of surfactant secretion and $[\text{Ca}^{2+}]_{\text{cyt}}$ were in direct dependency of intraalveolar CO_2 concentration. To elucidate whether the calcium shift from the cytosol to the mitochondria was responsible for the reduction of surfactant secretion during hypocapnia we first tested if surfactant secretion was promoted by calcium. Therefore, we intraalveolarly infused the intracellular Ca^{2+} chelator BAPTA-AM and repeated the measurement of LTG fluorescence intensity under hypercapnic conditions. We could show that the hypercapnia-induced acceleration of surfactant secretion was blocked and the LTG fluorescence intensity values were similar to those under normocapnic conditions (figure 5C). Secondly, we pretreated the alveolar epithelial cells with the mitochondrial inhibitor rotenone. This procedure blocked the hypocapnia-induced reduction of surfactant secretion (figure 5C). Furthermore, the rate of surfactant secretion under these conditions was similar to that under control conditions (figure 5C).

Hypocapnia reduces alveolar ventilation *in situ*. To elucidate the effect of hypocapnia-induced reduction of the surfactant secretion on the alveolar ventilation we performed bright field microscopy of a specific lung area at baseline and two hours of exposition with normcapnia (40 mmHg p CO_2) or hypocapnia (<10 mmHg p CO_2). Hypocapnia reduced the projected alveolar area by 21% compared to their normocapnia state. In contrast, in rotenone-pretreated alveoli hypocapnia had no effect on the projected alveolar area (figure 5D and E).

Ligature of pulmonary artery reduces surfactant protein D-secretion and alveolar surface in White New Zealand Rabbits *in vivo*. Intravital microscopy of the lung surface of volume-controlled ventilated rabbits revealed that following pulmonary artery ligation for 2 hours the projected alveolar surface area decreased by about 30%. In contrast, inspiratory CO_2 admixture inhibited this decrease of the projected alveolar surface area (figure 6A and B). In accordance with this observations surfactant protein D concentration in the BAL

decreased in lungs with ligated pulmonary arteries. This response was inhibited by 5% CO₂ ventilation (figure 6C and D).

Ligation of pulmonary artery reduces the compliance and increase the inspiratory pressure and the resistance and decreases the compliance in White New Zealand Rabbits *in vivo*. Ligation of pulmonary artery with consecutive intraalveolar hypocapnia induced an increase of the inspiratory pressure and the resistance and a decrease of the compliance vs. control *in vivo* (figure 6E-G). In contrast, all responses were inhibited by the inspiratory CO₂ admixture of 5% (figure 6E-G).

Discussion

We provide evidence that in isolated perfused rat lungs AEC sense changes in alveolar CO₂ concentration. When alveolar CO₂ decreases, as seen in non-perfused but ventilated alveoli, AEC respond with a mitochondrially triggered reduction of [Ca²⁺]_{cyt} and thus reductions in both LB exocytosis and alveolar ventilation (figure 7).

Pulmonary gas exchange failure might be associated with characteristic changes of [CO₂]_{iA}. In non-ventilated but perfused lung districts [CO₂]_{iA} might rise whereas lung areas without perfusion but with ventilation [CO₂]_{iA} declines¹⁹. Therefore, we hypothesized that in alveolar perfusion failure the drop in [CO₂]_{iA} provides the signal for AEC to reduce the alveolar ventilation in order to minimize ventilation/perfusion mismatch.

CO₂ sensing has been reported for plants and special types of neurons, as in brainstem and carotid body cells^{7,8}. Recently, Vadász *et al.* reported that isolated AEC respond to high CO₂ levels with a Ca²⁺-dependent activation of AMP-activated protein kinase and thus endocytosis of Na,K-ATPase²⁰. However, the mechanism by which CO₂ regulates Ca²⁺ signalling in AEC has not been elucidated so far.

Using our established real-time imaging of intact alveoli we could confirm *in situ* that [Ca²⁺]_{cyt} in AEC increases with elevated alveolar CO₂ levels. Furthermore, a decrease of [CO₂]_{iA} induced a reduction of [Ca²⁺]_{cyt}. The Ca²⁺ responses occurred in a direct relation to [CO₂]_{iA} within minutes in a totally reversible manner. The demonstration of CO₂-induced Ca²⁺ signalling in AEC constitutes to our knowledge the first reported real-time imaging of pulmonary AEC in the intact lung. Since we were not able to keep the pH constant in the alveolar epithelial lining fluid of the isolated lung following changing [CO₂]_{iA} we measured [Ca²⁺]_{cyt} in A549 cells under several conditions, in order to differentiate whether the Ca²⁺ responses in AEC were directly CO₂ rather than pH mediated. First, changing the CO₂ tension in the HEPES buffer from 40 to 0 or 80 mmHg and thus pH from 7.4 to 7.2 or 7.8, respectively, evoked a comparable [Ca²⁺]_{cyt} response to the *in situ* situation. Second, changing the CO₂ tension and keeping the pH constant at 7.4 induced the same [Ca²⁺]_{cyt} response. Third, pH change from 7.4 to 7.8 alone did not alter [Ca²⁺]_{cyt}. Furthermore, lowering CO₂ tension to 0 mmHg without additional pH buffering did not increase cytosolic pH. Taken together, these findings indicate that AEC sense CO₂ independently from pH.

To determine the underlying Ca²⁺-signalling mechanism, we considered the role of mitochondria, an important [Ca²⁺]_{cyt}-modifying cell organelle. Using the model of the isolated lung, we could demonstrate that hypocapnia was accompanied not only by a decrease of [Ca²⁺]_{cyt} but also by an increase of [Ca²⁺]_{mito}. Its measurement was based on cationic rhod 2 that accumulates in the anionic mitochondrial matrix. Cytosolic localisation could reduce the specificity for the determination of [Ca²⁺]_{mito}. To keep this error small we co-localized the rhod 2 fluorescence with the specific dye MTG. Furthermore, Ichimura and coworkers were able to demonstrate using a similar experimental setup that cell permeabilization revealed a quick release of the mainly cytosolic-localized fura 2 whereas the rhod 2 fluorescence stayed constant indicating that rhod 2 was mainly in the cytosol²¹⁻²⁴. In our case, hypocapnia induced a contrary change of [Ca²⁺] in the cytosol or in the mitochondria. Since we cannot completely exclude cytosolic localization of rhod 2 our determined [Ca²⁺]_{mito} increase might therefore be underestimated. Additionally, we could show that the [Ca²⁺]_{cyt} response was inhibited by the blockade of the mitochondrial Ca²⁺ uniporter with ruthenium red or the complex 1 with rotenone indicating a Ca²⁺ shift from the cytosol into mitochondria. The inhibitory effect of ruthenium red was less effective than of rotenone, which can be explained

by their different cell permeability characteristics. Summarizing these findings we suggest that hypocapnia induced a Ca^{2+} shift from the cytosol to the mitochondria.

The decrease of $[\text{Ca}^{2+}]_{\text{cyto}}$ following lowering $[\text{CO}_2]_{\text{iA}}$ could also be explained by a Ca^{2+} shift into the extracellular space or endoplasmic reticulum (ER). One could consider that rotenone, as a complex 1 inhibitor, might suppress ATP production and thus the Ca^{2+} -ATPase dependent Ca^{2+} shift to the extracellular or ER compartment. Since, in contrast to rotenone, ruthenium red does not directly inhibit the respiratory chain and thus ATP production we believe that the inhibitory effect on the decrease of $[\text{Ca}^{2+}]_{\text{cyto}}$ following hypocapnia was mainly due to an inhibition of mitochondrial Ca^{2+} uptake. Furthermore, the hypocapnia-induced ER uptake of Ca^{2+} could be ruled out because fura 2ff ratio did not change after lowering CO_2 (data not shown).

The inhibition of the CO_2 -induced Ca^{2+} shift by rotenone further suggests that the driving force for the mitochondrial Ca^{2+} uptake was an increase of the respiratory chain activity and hence transmembrane potential. This hypothesis was confirmed by the finding that the fluorescence of TMRM, which accumulates in mitochondria in a potential-dependent manner, was enhanced in A549 cells under hypocapnic conditions compared to normocapnic conditions^{25,26}. Addition of rotenone revealed a quick decrease of the TMRM fluorescence indicating that the respiratory chain activity is the important determinant of mitochondrial transmembrane potential. Further, hypocapnia induced an increase of the respiratory chain substrate NADH and the knockdown of isocitrate dehydrogenase, the NADH-producing Krebs cycle enzyme, inhibited the decrease of $[\text{Ca}^{2+}]_{\text{cyto}}$ under low CO_2 levels. The dependency of the respiratory chain activity from NADH has been demonstrated by Kuznetsov *et al.*²⁷. Hence, in hypocapnia, NADH production and thus transmembrane potential, the driving force for the mitochondrial Ca^{2+} uptake, is increased. We therefore suggest that CO_2 , a byproduct of the Krebs cycle, inhibits Krebs cycle activity in a negative feedback loop. Under hypocapnic conditions, this inhibitory effect of CO_2 on the Krebs cycle activity is reduced which subsequently increases NADH production and in turn the mitochondrial transmembrane potential.

Under hypocapnic conditions, the $[\text{Ca}^{2+}]_{\text{cyt}}$ decrease was associated with a reduction of LB secretion. In contrast, the hypercapnia-induced increase of $[\text{Ca}^{2+}]_{\text{cyt}}$ was related to an increase in LB secretion. This response was completely blocked by the cytosolic Ca^{2+} chelator BAPTA indicating that CO_2 regulates LB secretion in a Ca^{2+} -dependent manner. Although Ca^{2+} independent exocytosis involving PKC- or cAMP-dependent mechanisms might occur, Ca^{2+} as a critical stimulus for LB secretion has been reported by several authors. For instance, Ichimura *et al.* demonstrated that Ca^{2+} uncaging stimulates LB secretion⁴. Furthermore, in cultured Type 2 cells, an increase in $[\text{Ca}^{2+}]_{\text{cyt}}$ induced by ionophores, cell stretch, or by secretagogues evoked surfactant secretion^{5,6}. However, the role of CO_2 on Ca^{2+} -mediated LB secretion has so far not been elucidated. It has been reported that in lipopolysaccharide (LPS) treated Type 2 cells co-cultured with alveolar macrophages surfactant secretion did not change under hypercapnic conditions. Since surfactant responses to CO_2 were not measured in the absence of LPS it is not clear whether CO_2 was ineffective or the LPS inhibited a hypothetical CO_2 -mediated alteration in surfactant secretion²⁸. Shepard and colleagues measured the volumetric density of LB in response to CO_2 in isolated and ventilated dog lungs²⁹. The authors demonstrated that the LB density decreased at low CO_2 tension. However, the responsible cellular processes in terms of LB synthesis, secretion and/or reabsorption were not determined. Other potential aspects are that CO_2 might influence alveolar ventilation and that ventilation stimulates surfactant secretion³⁰. Therefore, it is not clear whether the LB density responses observed were due to CO_2 or ventilation.

During hypocapnia rotenone blocked not only the Ca^{2+} shift from the cytosol to the mitochondria but also the inhibition of LB secretion. We therefore conclude that mitochondria regulate LB secretion by modifying $[\text{Ca}^{2+}]_{\text{cyt}}$ in a CO_2 -dependent fashion because cytosolic Ca^{2+} chelation abolished LB secretion. Since rotenone had no effect on $[\text{Ca}^{2+}]_{\text{cyt}}$ or on LB secretion under normocapnic conditions (data not shown) we rule out direct interference of rotenone with the LB secretion process. It is known that rotenone inhibits the mitochondrial membrane potential and thus ATP production. ATP as a paracrine mediator induces surfactant secretion by ligating purinergic receptors³¹. In our experiments this mechanism, however, does not play a relevant role because LB secretion was enhanced and not inhibited following rotenone. ATP is also required for the endoplasmic Ca^{2+} uptake evoked by Ca^{2+} ATPase. A potential influence of rotenone on LB secretion through inhibition of endoplasmic Ca^{2+} uptake is also unlikely because $[\text{Ca}^{2+}]_{\text{cyt}}$ did not change after rotenone.

Similar to LB secretion, the mean projected alveolar area decreased during hypocapnia and was also blocked by rotenone. Since surfactant reduces alveolar surface tension, it is likely that at constant alveolar pressure, as given in our experiments, the hypocapnia-induced reduction of the alveolar projected area was directly caused by the decrease of LB secretion. Tsang *et al.* showed in piglets that an acute pulmonary thrombembolism causes a compensatory ventilation shift out of non-perfused lung regions which is initiated by a hypocapnia-induced bronchoconstriction¹⁹. We assume that in our model bronchoconstriction is not of significant relevance because rotenone, which was administered directly into to alveolus by bypassing the regarding bronchioli, inhibited the hypocapnia-induced reduction of the projected alveolar area. It is important to consider that the buffer in which rotenone is dissolved interacts with the alveolar lining fluid. Thus, alveoli from the comparison groups were also treated with the vehicle. However, the potential buffer-induced dilution of surfactant might counter the inhibitory effect of rotenone. We point out that our interpretations are limited to a two-dimensional analysis of a three-dimensional alveolar geometry. Nevertheless, assuming a spherical shape of alveoli changes of the projected area would be signify even higher changes in alveolar volume. Therefore, the measurement of the projected alveolar area might underrepresent the alveolar ventilation. Taken together, our findings provide the first evidence that mitochondria regulate LB secretion and thus alveolar ventilation in a CO_2 -dependent manner.

To test whether the hypocapnia-induced reduction of LB secretion and as a consequence alveolar ventilation is a relevant mechanism in alveolar perfusion failure in order to minimize ventilation/perfusion mismatch, we carried out *in vivo* experiments with intravital lung microscopy and pulmonary artery ligation. In accordance with the *in situ* findings the occlusion of the pulmonary artery resulted in a decrease of the projected alveolar area indicating a reduction of ventilation in the non-perfused lung area. This finding confirms reports by several authors. Bruns and Sauerbruch were probably the first who in 1911 described that the ligation of a pulmonary artery branch in dogs resulted in a collapse of the corresponding pulmonary lobe³². In 2009 Tsang *et al.* reported that alteration of regional CO_2 tension correlates with the changes of regional ventilation¹⁹. As described above, the authors considered that a hypocapnia-induced bronchoconstriction was responsible for the ventilation reduction. We cannot exclude this mechanism in our experiments. However, we found that the decrease in alveolar ventilation following pulmonary artery ligation was accompanied by a reduction of the surfactant protein concentration in the BAL and that these responses were inhibited by adding CO_2 into the inspired gas. Since surfactant reduces alveolar surface tension we conclude that this mechanism plays at least a partial role in adapting ventilation to changes in perfusion.

In summary, we identify a novel CO₂-sensing mechanism of AEC in which mitochondria play a key role. The functional consequence is a Ca²⁺-mediated regulation of LB secretion. We conclude that this mechanism regulates the reduction of ventilation in lung areas with perfusion failure in order to reduce ventilation/perfusion mismatch and thus optimize gas exchange.

Acknowledgements

We thank Monika Weber, Kirsten Pfeiffer-Drenkhahn, Claudia Lüchau, and Sonja Schuppart for their excellent technical assistance and Andrew Bacelis for proofreading.

Author contribution

All authors contributed extensively to the work presented in this paper.

Figure legends

Figure 1. $[Ca^{2+}]_{cyt}$ in alveolar epithelial cells *in situ*. (A) Images of a single intact alveolus show the pseudocolor-coded 340:380 ratio for fura 2-loaded alveolar epithelial cells normocapnic ($[CO_2]_{iA}$: 5 Vol%), hypocapnic ($[CO_2]_{iA}$: 0 Vol%), and hypercapnic ($[CO_2]_{iA}$: 10 Vol%) conditions. Alveolar septum is indicated (arrows). (B) Tracing of $[Ca^{2+}]_{cyt}$ (gray) and the mean value (black) of the respective oscillation minimum and maximum from an identical epithelial cell under normo-, hypo and hypercapnic conditions. Intraalveolar hypocapnia reduces $[Ca^{2+}]_{cyt}$ by 40 nM whereas hypercapnia increases $[Ca^{2+}]_{cyt}$ by 45 nM *in situ*. Regarding $[CO_2]_{iA}$ were as indicated. (C) Group data of $[Ca^{2+}]_{cyt}$ -responses 15 minutes following onset of hypo- or hypercapnic conditions with $[CO_2]_{iA}$ of 0 or 10 Vol% CO_2 , respectively. Mean \pm SE, # $p < 0.05$ vs. $[CO_2]_{iA}$ of 5 Vol%. Repeated 5 times. (D) Alveolar microinjection the mitochondrial inhibitors ruthenium red or rotenone inhibited the hypocapnic ($[CO_2]_{iA}$: 0 Vol%)-induced reduction of $[Ca^{2+}]_{cyt}$ by 50 or 100%, respectively, *in situ*. Mean \pm SE, # $p < 0.05$ vs. 5 Vol% $[CO_2]_{iA}$. Repeated 5 times.

Figure 2. $[Ca^{2+}]_{mito}$ in alveolar epithelial cells *in situ*. (A) Images show the identical alveolus loaded with the specific mitochondrial dye MTG (green fluorescence) in combination with the calcium sensitive dye rhod 2 (red fluorescence) and the computer-generated co-localization of both dyes (yellow). Arrows indicate mitochondria. Dotted lines are alveolar margins as detected in bright-field images obtained in parallel. (B) Group data analysis of rhod 2 fluorescence in AEC of an intact alveolus under normo- and hypocapnic conditions ($[CO_2]_{iA}$ of 5 or 0 Vol%, respectively), mean \pm SE, n=6.

Figure 3. $[Ca^{2+}]_{cyt}$ -response to CO_2 in dependence of pH *in vitro*. (A) Tracing of $[Ca^{2+}]_{cyt}$ in A549 cells under normo- and hypocapnic conditions. Black blot: the pH of the superfusion buffer was 7.4 under normocapnic conditions and increased to 7.8 under hypocapnic conditions. Red blot: the pH of the superfusion buffer was kept constant at 7.4 even under hypocapnic conditions. (B) Bars show group data of $[Ca^{2+}]_{cyt}$ in A549 cells for indicated superfusion conditions. Hypocapnia induced a reduction of $[Ca^{2+}]_{cyt}$ under constant extracellular pH of 7.4, whereas a change of extracellular pH from 7.4 to 7.8 did not change $[Ca^{2+}]_{cyt}$ under normocapnic conditions *in vitro*. Mean \pm SE, # $p < 0.05$ vs. baseline. Repeated 8 times. (C) Cytosolic pH calibration: cytosolic 500:450 ratio for BCECF-loaded A549 cells treated with 0.005% saponin for 1 minute followed by superfusion with buffer at given pH values. Mean \pm SE, $r = 0.47$, repeated twice. (D) Cytosolic pH in BCECF-loaded A549 cells under normo- or hypocapnic conditions, as indicated. Extracellular pH changed from 7.4 under normocapnic to 7.8 under hypocapnic conditions. Repeated 7 times.

Figure 4. $[Ca^{2+}]_{cyt}$, $[Ca^{2+}]_{mito}$, NADH, and $\Delta\Psi$ in alveolar epithelial cells *in situ*. (A) Tracing of the ratio between mitochondrial and cytosolic TMRM fluorescence intensity of native, scrambled siRNA- or IDH3G- siRNA-treated A549 cells under normo- or hypocapnic conditions at constant pH of 7.4, as indicated. (B) Group data of the TMRM ratio response 15 minutes following onset of hypocapnic conditions in native, scrambled siRNA- or IDH3G-siRNA-treated A549 cells at constant extracellular pH of 7.4, respectively. Mean \pm SE, # $p < 0.05$ vs. baseline, * $p < 0.05$ vs. native A549 cells. Repeated 4-6 times. (C) Tracing of the mitochondrial and cytosolic TMRM fluorescence intensity and the ratio between both of native, scrambled siRNA- or IDH3G- siRNA-treated A549 cells under normo- or hypocapnic

conditions, as indicated. Experiments were performed at constant extracellular pH of 7.4, respectively. Timepoint of rotenone application is marked by the arrow. **(D)** Group data of the TMRM ratio in native A549 cells before and after rotenone application, each under normocapnic condition, and after rotenone under hypocapnic conditions. Experiments were performed at constant extracellular pH of 7.4, respectively. Mean±SE, # p<0.05 vs. normocapnia without rotenone. Repeated 5 times. **(E)** Gels show RT-PCR products for IDH3G- and GAPDH-mRNA in native (lane 2 and 3), in IDH3G siRNA- (lane 4 and 5), and scrambled siRNA-treated (lane 6 and 7) A549 cells. Lane 1 and 8: molecular weight ladder. **(F)** Group data of $[Ca^{2+}]_{cyt}$ -responses 10 minutes following onset of hypocapnic conditions at constant extracellular pH of 7.4 in native, scrambled siRNA- or IDH3G-siRNA-treated A549 cells. Mean±SE, * p<0.05 vs. native A549 cells, § p<0.05 vs. scrambled siRNA-treated A549 cells. Repeated 6 times. **(G)** Tracing of rhod 2 fluorescence of native, scrambled siRNA- or IDH3G- siRNA-treated A549 cells under normo- or hypocapnic conditions, as indicated. Experiments were performed at constant extracellular pH of 7.4, respectively. **(H)** Group data of rhod 2 fluorescence response 10 minutes following onset of hypocapnic conditions in native, scrambled siRNA- or IDH3G-siRNA-treated A549 cells. Experiments were performed at constant extracellular pH of 7.4, respectively. Mean±SE, * p<0.05 vs. native A549 cells, § p<0.05 vs. scrambled siRNA-treated A549 cells. Repeated 6 times. **(I)** Group data of NADH-concentration measured by a NADH-assay in native A549 under normocapnic conditions, hypocapnic conditions and after rotenone under hypocapnic conditions at constant extracellular pH of 7.4, respectively. Mean±SE, * p<0.05 vs. normocapnia, § p<0.05 vs. hypocapnia alone. Repeated 8 times. **(J)** Tracing of rhod 2 fluorescence of native or IDH3G-siRNA-treated A549 cells under normo- or hypocapnic conditions, as indicated. Rotenone was applied after baseline in both groups. Experiments were performed at constant extracellular pH of 7.4, respectively. **(K)** Group data of NADH response 10 minutes following rotenone alone and 10 minutes following rotenone in combination with hypocapnic conditions in native or IDH3G-siRNA-treated A549 cells. Experiments were performed at constant extracellular pH of 7.4, respectively. Mean±SE, # p<0.05 vs. baseline. Repeated 6 times.

Figure 5. Surfactant secretion in AEC *in situ*. **(A)** Image shows an LTG-loaded alveolus. Arrows indicate lamellar bodies from alveolar Type 2 cells. Dotted lines are alveolar margins as detected in bright-field images obtained in parallel. **(B)** Color-coded images of a single alveolar type II cell after alveolar microinjection of LysoTracker Green (LTG). Pictures were taken under baseline conditions with an alveolar CO₂ concentration of 5 Vol% and 20 minutes after switching to 0 or 10 Vol% or staying at 5 Vol%. **(C)** Time dependency of LTG-intensity. Data are mean±SE. LTG-intensity decreases equivalent to constant surfactant secretion under normocapnic conditions. Hypocapnia induces an inhibition of the surfactant secretion, whereas hypercapnia increases the surfactant secretion *in situ*. Hypocapnia-induced reduction of surfactant secretion is blocked by rotenone microinjected into the alveolus. Hypercapnia-induced elevation of surfactant secretion is blocked by BAPTA microinjected into the alveolus. * p<0.05 vs. 5 Vol% [CO₂]_{iA}. Repeated 6 times. **(D)** Brightfield image of the isolated lung surface under baseline conditions and 120 min after intervention as indicated. **(E)** Hypocapnia of 0 Vol% [CO₂]_{iA} reduces the projected alveolar area up to about 21% vs. 5 Vol% [CO₂]_{iA} after 2 hours of exposition *in situ*. Hypocapnia has no effect on the projected alveolar area in rotenone-pretreated alveoli. Data are mean±SE. # p<0.05 vs. 5 Vol% [CO₂]_{iA}. Repeated 6 times.

Figure 6. Ventilation after pulmonary artery ligation *in vivo*. (A) Intravital brightfield image of the lung surface. Microscopy was performed through a thoracic window implanted into the left chest wall of a rabbit. Pictures were taken under baseline conditions and 120 minutes following sham dissection (control) or ligation of the ipsilateral pulmonary artery with or without 5 Vol% CO₂ insufflation. (B) Group data of the projected alveolar perimeter under baseline conditions and 120 minutes following sham dissection (control) or ligation of the ipsilateral pulmonary artery (PA-ligation) without or with 5 Vol% CO₂ insufflation. Data are means±SE, * p<0.05 vs. control, § p<0.05 vs. PA-ligation+CO₂. Repeated 4 times. (C) Representative Western blot of SP-D in rabbit BAL. Lane 1: molecular weight ladder, lane 2 and 3: control, lane 4: PA-ligature, lane 5 and 6: CO₂ insufflation + PA-ligature. (D) Groupdata analysis of SP-D density, data are means ± SEM. * p < 0.05% vs. sham. (E-G) Groupdata analysis of p_{insp}, resistance or compliance under baseline conditions and 120 minutes following sham dissection (control) or ligation of the ipsilateral pulmonary artery with or without CO₂ insufflation. Data are means ± SEM. * p < 0.05% vs. control, § p < 0.05 vs. PA-ligature + 5 Vol% CO₂. Repeated 4 times.

Figure 7. (A) Pulmonary perfusion failure leads to a decrease of [CO₂]_{iA}. This [CO₂]_{iA} drop is sensed by alveolar epithelial cells resulting in a reduction of alveolar ventilation and thus ventilation/perfusion mismatch. (B) Sequence of events underlying Ca²⁺ dependent [CO₂]_{iA} sensing mechanism. Alveolar perfusion failure leads to alveolar hypocapnia (I). Alveolar hypocapnia induced activation of Krebs cycle via a feedback mechanism (II). Krebs cycle activation induces via an increase of NADH (III) an elevation of ΔΨ (IV) with following calcium shift from cytosol into the mitochondrium (V). Decrease of [Ca²⁺]_{cyt} results in a reduction of Ca²⁺ dependent surfactant secretion (VI).

Methods

Animals. Male Sprague Dawley rats (350g) and White New Zealand rabbits (2.5 kg) were purchased from Charles River (Sulzfeld, Germany) (see supplementary methods for details).

Materials. Fura 2-AM, LysoTracker green (LTG), MitoTracker green (MTG), rhod 2, BCECF-AM (2', 7'-bis-(2-carboxymethyl)-5-(and 6-) carboxyfluorescein-AM) and TMRM (tetramethylrhodamine methyl ester) were purchased from Molecular probes (Invitrogen, Karlsruhe, Germany). Rotenone, ruthenium red and BAPTA-AM (1, 2-bis-(2-aminophenoxy)-ethane-N, N, N', N'-tetraacetic acid tetrakis-(acetoxymethylester)) were purchased from Sigma-Aldrich (Germany). Vehicle for dyes and other agents was HEPES buffer (150 mmol/l Na⁺, 5 mmol/l K⁺, 1.0 mmol/l Ca²⁺, 1 mmol/l Mg²⁺, and 20 mmol/l HEPES at pH 7.4) containing 4% dextran (70 kDa) and 1% FBS at pH 7.4 and osmolarity of 295 mosm. All esterified fluorescent probes were prepared as stock solutions in dimethylsulfoxide (DMSO).

In situ experiments

Lung preparation. Using the previously reported method, lungs were isolated from Sprague-Dawley rats (anesthetized with 1.2 Vol% isoflurane and intraperitoneal injection of 100 mg/kg ketamine and 20 mg/kg xylazine (rompunTM)), and perfused with autologous blood (14ml/min) at 37°C^{33,34}. Lungs were constantly inflated through an airway cannula with an airway pressure of 5 cmH₂O with a normocapnic gas mixture of 30% O₂, 5% CO₂, and 65% N₂ under baseline conditions. Pulmonary artery and left atrial (P_{LA}) pressures were held at 10 and 2 cmH₂O, respectively.

Alveolar micropuncture. We gave intraalveolar injections by alveolar micropuncture according to previously reported methods^{4,34,35} (see supplementary for details).

Hypocapnia/hypercapnia induction. Switching the inflation gas to a hypocapnic (30% O₂, 0% CO₂ and, 70% N₂) or hypercapnic (30% O₂, 10% CO₂ and, 60% N₂) mixture altered the pCO₂ of the venous blood to hypocapnic values from 36.8±6.5 to 6.6±2.3 mmHg or to 79.6±3.6 mmHg, respectively. Blood pO₂ was constant throughout (215±34 mmHg). To prevent CO₂-diffusion to the ambient air across the exposed lung surface, we covered the lungs with gas-tight plastic.

Real-time lung imaging. Using an epifluorescence microscope (Axiovert, Zeiss, Göttingen, Germany) fluorophores were excited using appropriate interference filters and filter sets (Semrock, Rochester, USA) (see supplementary methods for details).

Alveolar [Ca²⁺]_{cyt} and [Ca²⁺]_{mito} determinations. Our methods for [Ca²⁺]_{cyt} and [Ca²⁺]_{mito} quantification were previously described^{34,36-38}. Briefly, we quantified [Ca²⁺]_{cyt} in alveolar epithelial cells by the fura 2 method after alveolar microinjection of fura 2-AM for 30 min. To detect [Ca²⁺]_{mito} we microinjected rhod 2-AM into an alveolus for 15min followed by a Ringer's flush (see supplementary methods for details).

Alveolar Type II cell exocytosis of surfactant. To determine surfactant secretion *in situ*, we imaged single alveolar cells from isolated blood-perfused rat lung through the loss of cell fluorescence of intraalveolar microinjected LysoTracker Green (LTG)³⁵.

Measurement of alveolar projected area. To measure the influence of altered surfactant secretion through hypocapnia ([CO₂]_{iA} <10mmHg), we took light microscopy pictures of the

lung surface with 20x amplification and measured the size of the projected alveolar area by using the software Metamorph (Molecular Device; Downington, PA, USA).

Experimental protocol. $[Ca^{2+}]_{\text{cyt}}$, $[Ca^{2+}]_{\text{mito}}$, surfactant secretion, and alveolar projected area were measured under normocapnic and hypocapnic conditions. To identify the supposed key role of the mitochondria, we microinjected ruthenium red or rotenone and repeated the measurement of $[Ca^{2+}]_{\text{cyt}}$, $[Ca^{2+}]_{\text{mito}}$, surfactant secretion, and alveolar projected area under normocapnic and hypocapnic conditions in an additional set of experiments. To elucidate the Ca^{2+} -dependency of surfactant secretion, the membrane-permeating Ca^{2+} chelator BAPTA-AM in Ca^{2+} -free buffer (150 mmol/l Na^+ , 5 mmol/l K^+ , 1 mmol/l Mg^{2+} , and 20 mmol/l HEPES at pH 7.4) was microinjected and surfactant secretion, and alveolar projected area was determined under normocapnic and hypocapnic conditions.

***In vitro* experiments**

Cell culture. Human lung carcinoma A549 cells with type 2 cell characteristics were grown in F-12K Medium (ATCC, Mahassa, VA, USA). This cell type has been widely used as a model to study the response of AEC in several conditions^{39,40} (see supplementary methods for details).

Real-time cell imaging. For fluorescent imaging of fluorophore-loaded cells an epifluorescence microscope (Olympus, Germany) was used (see supplementary methods for details).

$[Ca^{2+}]_{\text{cyt}}$ determinations. For $[Ca^{2+}]_{\text{cyt}}$ measurements, cells were loaded for 45 minutes with 10 μ M fura-2-AM. Fluorescence images were recorded under normo- or hypocapnic conditions in combination with an extracellular pH of 7.4 or 7.8 at 10 seconds intervals (see supplementary methods for details).

Cytosolic pH measurement. Cells were loaded with the acetoxymethyl esters of BCECF (5 mM)⁴¹. Cytosolic pH was measured after induction of hypocapnia (<10 mmHg pCO₂) (see supplementary methods for details).

Mitochondrial membrane potential measurement. For mitochondrial membrane potential assessment, A549 cells were loaded with tetramethylrhodamine methyl ester (TMRM). This indicator dye is a lipophilic cation accumulated by mitochondria in proportion to the electrical potential across their inner membrane ($\Delta\psi$)⁴². The wavelength for excitation was 560 nm while monitoring the emission at 590 nm. Addition of the mitochondrial depolarizer FCCP (50 nM) resulted in a rapid loss of the mitochondrial TMRM fluorescence.

Mitochondrial NADH production. NADH concentration was quantified by measuring its autofluorescence intensity. A549 were excited with 360 nm while monitoring the emission at 510 nm. For proofing the mitochondrial production of NADH, its autofluorescence was co-localized with the mitochondria specific marker MTG.

Biochemical determination of NADH concentration. The NADH concentrations in cells are measured using the ultrasensitive EnzyChrom TM NAD⁺/NADH Assay Kit from BioAssay Systems (Hayward, CA, USA) (see supplementary methods for details).

Isocitrate dehydrogenase 3 (NAD⁺ gamma (IDH3G) knockdown. A549 cells were transfected with 10 nM stealth siRNA of IDH3G (Invitrogen and control (scrambled) stealth siRNA (Invitrogen) by using Lipofectamine RNAiMAX (Invitrogen) according to the manufacturer's protocol (see supplementary methods for details).

Reverse transcriptase polymerase chain reaction (RT-PCR). (see supplementary methods for details).

In-vivo experiments

Lung preparations. White male New Zealand rabbits were anesthetized by intravenous application of midazolam (0.1 mg/kg), fentanyl (5 µg/kg) and pancuronium bromide (0.3 mg/kg bw). The surgical preparation and experimental setup have previously been described in detail^{43,44} (see supplementary methods for details).

Intravital microscopy. Subpleural alveoli were sequentially visualized under a fluorescence microscope (Zeiss, AxioTech, Germany) during prolonged inspiration periods of 10 seconds. For video recordings a CCD camera (Photometrics Coolsnap HQ², USA) and Metamorph software (Molecular Device; Downingtown, PA, USA) were used.

Measurement of alveolar projected area. To measure the influence of altered surfactant secretion through hypocapnia we took light microscopy pictures of the lung surface with 20x amplification and measured the size of the projected alveolar area by using the software Metamorph (Molecular Device; Downingtown, PA, USA).

Experimental protocol. The rabbits were randomized into three groups: 1. control without pulmonary artery ligature (control-group), 2. pulmonary artery ligature (PA-ligature group), 3. pulmonary artery ligature with inspiratory application of CO₂ (therapy-group). Compliance, resistance and inspiratory pressure were measured by the respirator (Zeus[®], Dräger, Lübeck, Germany) and changes in projected alveolar area were visualized by light microscopy at baseline and after 120 minutes. At the end of videomicroscopy the animals were sacrificed and the lungs were lavaged for the measurement of the surfactant protein A-fraction by westernblotting.

Western blot. (see supplementary methods for details).

Statistics

All data are represented as means ± SE. Statistical data analysis was performed using SigmaStat (Systat Software, USA). Comparisons between the groups were tested using ANOVA on ranks followed by a pairwise multiple comparison. Repeated measurements were tested using the Mann-Whitney Rank Sum Test. Statistical significance was accepted at p<0.05.

References

1. Moore,R.L., Humphreys,G.H., & Cochran,H.W. The effect of sudden occlusion of either primary pulmonary artery on cardiac output and pulmonary expansion. *J. Thorac. Surg.* **3**, 573-589 (1934).
2. Venrath, H., Rotthoff,F., Valentin,H., & Bolt,W. [Bronchspirometry in vascular diseases of the minor circulation.]. *Beitr. Klin. Tuberk. Spezif. Tuberkuloseforsch.* **107**, 291-294 (1952).
3. Swenson,E.W., Finley,T.N., & Guzman,S.V. Unilateral hypoventilation in man during temporary occlusion of one pulmonary artery. *J. Clin. Invest* **40**, 828-835 (1961).
4. Ichimura,H., Parthasarathi,K., Lindert,J., & Bhattacharya,J. Lung surfactant secretion by interalveolar Ca²⁺ signaling. *Am. J Physiol Lung Cell Mol. Physiol* **291**, L596-L601 (2006).
5. Mescher,E.J., Dobbs,L.G., & Mason,R.J. Cholera toxin stimulates secretion of saturated phosphatidylcholine and increases cellular cyclic AMP in isolated rat alveolar type II cells. *Exp. Lung Res.* **5**, 173-182 (1983).
6. Sano,K., Voelker,D.R., & Mason,R.J. Effect of secretagogues on cytoplasmic free calcium in alveolar type II epithelial cells. *Am. J Physiol* **253**, C679-C686 (1987).
7. Young,J.J. *et al.* CO(2) signaling in guard cells: calcium sensitivity response modulation, a Ca(2+)-independent phase, and CO(2) insensitivity of the *gca2* mutant. *Proc. Natl. Acad. Sci. U. S. A* **103**, 7506-7511 (2006).
8. Summers,B.A., Overholt,J.L., & Prabhakar,N.R. CO(2) and pH independently modulate L-type Ca(2+) current in rabbit carotid body glomus cells. *J Neurophysiol.* **88**, 604-612 (2002).
9. Ichas,F., Jouaville,L.S., & Mazat,J.P. Mitochondria are excitable organelles capable of generating and conveying electrical and calcium signals. *Cell* **89**, 1145-1153 (1997).
10. Babcock,D.F. & Hille,B. Mitochondrial oversight of cellular Ca²⁺ signaling. *Curr. Opin. Neurobiol.* **8**, 398-404 (1998).
11. Jouaville,L.S., Ichas,F., & Mazat,J.P. Modulation of cell calcium signals by mitochondria. *Mol. Cell Biochem.* **184**, 371-376 (1998).
12. Babcock,D.F., Herrington,J., Goodwin,P.C., Park,Y.B., & Hille,B. Mitochondrial participation in the intracellular Ca²⁺ network. *J Cell Biol* **136**, 833-844 (1997).
13. Starkov,A.A. The molecular identity of the mitochondrial Ca²⁺ sequestration system. *FEBS J* **277**, 3652-3663 (2010).
14. Chinopoulos,C. & dam-Vizi,V. Mitochondrial Ca²⁺ sequestration and precipitation revisited. *FEBS J* **277**, 3637-3651 (2010).
15. Brown,G.C. Control of respiration and ATP synthesis in mammalian mitochondria and cells. *Biochem. J* **284 (Pt 1)**, 1-13 (1992).

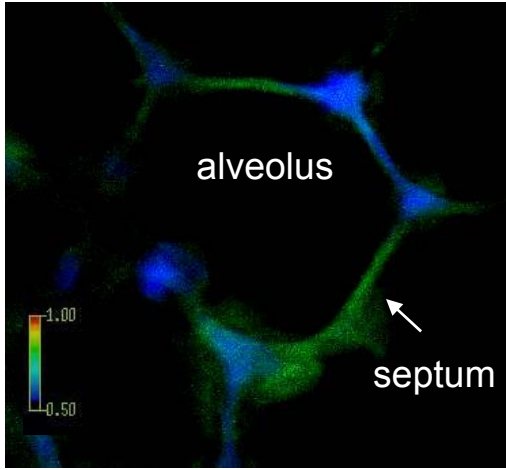
16. Erecinska,M. & Wilson,D.F. Regulation of cellular energy metabolism. *J Membr. Biol* **70**, 1-14 (1982).
17. Erecinska,M., Wilson,D.F., & Nishiki,K. Homeostatic regulation of cellular energy metabolism: experimental characterization in vivo and fit to a model. *Am. J Physiol* **234**, C82-C89 (1978).
18. Kaftan,E.J., Xu,T., Abercrombie,R.F., & Hille,B. Mitochondria shape hormonally induced cytoplasmic calcium oscillations and modulate exocytosis. *J Biol Chem.* **275**, 25465-25470 (2000).
19. Tsang,J.Y., Lamm,W.J., & Swenson,E.R. Regional CO₂ tension quantitatively mediates homeostatic redistribution of ventilation following acute pulmonary thromboembolism in pigs. *J. Appl. Physiol* **107**, 755-762 (2009).
20. Vadasz,I. *et al.* AMP-activated protein kinase regulates CO₂-induced alveolar epithelial dysfunction in rats and human cells by promoting Na,K-ATPase endocytosis. *J. Clin. Invest* **118**, 752-762 (2008).
21. Ichimura,H., Parthasarathi,K., Quadri,S., Issekutz,A.C., & Bhattacharya,J. Mechano-oxidative coupling by mitochondria induces proinflammatory responses in lung venular capillaries. *J. Clin. Invest* **111**, 691-699 (2003).
22. Kim,B. & Matsuoka,S. Cytoplasmic Na⁺-dependent modulation of mitochondrial Ca²⁺ via electrogenic mitochondrial Na⁺-Ca²⁺ exchange. *J Physiol* **586**, 1683-1697 (2008).
23. Koopman,W.J., Distelmaier,F., Esseling,J.J., Smeitink,J.A., & Willems,P.H. Computer-assisted live cell analysis of mitochondrial membrane potential, morphology and calcium handling. *Methods* **46**, 304-311 (2008).
24. Andrienko,T.N., Picht,E., & Bers,D.M. Mitochondrial free calcium regulation during sarcoplasmic reticulum calcium release in rat cardiac myocytes. *J Mol. Cell Cardiol.* **46**, 1027-1036 (2009).
25. Penzo,D. *et al.* Arachidonic acid released by phospholipase A(2) activation triggers Ca(2+)-dependent apoptosis through the mitochondrial pathway. *J Biol Chem.* **279**, 25219-25225 (2004).
26. Petronilli,V., Penzo,D., Scorrano,L., Bernardi,P., & Di,L.F. The mitochondrial permeability transition, release of cytochrome c and cell death. Correlation with the duration of pore openings in situ. *J Biol Chem.* **276**, 12030-12034 (2001).
27. Kuznetsov,A.V., Margreiter,R., Amberger,A., Saks,V., & Grimm,M. Changes in mitochondrial redox state, membrane potential and calcium precede mitochondrial dysfunction in doxorubicin-induced cell death. *Biochim. Biophys. Acta*(2011).
28. Dixon,D.L., Barr,H.A., Bersten,A.D., & Doyle,I.R. Intracellular storage of surfactant and proinflammatory cytokines in co-cultured alveolar epithelium and macrophages in response to increasing CO₂ and cyclic cell stretch. *Exp. Lung Res.* **34**, 37-47 (2008).
29. Shepard,J.W., Jr., Dolan,G.F., & Yu,S.Y. Factors regulating lamellar body volume density of type II pneumocytes in excised dog lungs. *J Appl. Physiol* **53**, 555-562 (1982).

30. Faridy,E.E. Effect of distension on release of surfactant in excised dogs' lungs. *Respir. Physiol* **27**, 99-114 (1976).
31. Dietl,P., Liss,B., Felder,E., Miklavc,P., & Wirtz,H. Lamellar body exocytosis by cell stretch or purinergic stimulation: possible physiological roles, messengers and mechanisms. *Cell Physiol Biochem.* **25**, 1-12 (2010).
32. Bruns,O. & Sauerbruch,F. *Mitt. a. d. Grenzgeb. d. Med. u. Chir.* **23**, 343 (1911).
33. Kiefmann,R., Rifkind,J.M., Nagababu,E., & Bhattacharya,J. Red blood cells induce hypoxic lung inflammation. *Blood* **111**, 5205-5214 (2008).
34. Kiefmann,R., Islam,M.N., Lindert,J., Parthasarathi,K., & Bhattacharya,J. Paracrine purinergic signaling determines lung endothelial nitric oxide production. *Am. J. Physiol Lung Cell Mol. Physiol* **296**, L901-L910 (2009).
35. Ashino,Y., Ying,X., Dobbs,L.G., & Bhattacharya,J. [Ca(2+)](i) oscillations regulate type II cell exocytosis in the pulmonary alveolus. *Am. J. Physiol Lung Cell Mol. Physiol* **279**, L5-13 (2000).
36. Parthasarathi,K., Ichimura,H., Quadri,S., Issekutz,A., & Bhattacharya,J. Mitochondrial reactive oxygen species regulate spatial profile of proinflammatory responses in lung venular capillaries. *J Immunol.* **169**, 7078-7086 (2002).
37. Kuebler,W.M., Ying,X., Singh,B., Issekutz,A.C., & Bhattacharya,J. Pressure is proinflammatory in lung venular capillaries. *J. Clin. Invest* **104**, 495-502 (1999).
38. Poot,M. & Pierce,R.H. Detection of changes in mitochondrial function during apoptosis by simultaneous staining with multiple fluorescent dyes and correlated multiparameter flow cytometry. *Cytometry* **35**, 311-317 (1999).
39. Burvall,K., Palmberg,L., & Larsson,K. Metabolic activation of A549 human airway epithelial cells by organic dust: a study based on microphysiometry. *Life Sci.* **71**, 299-309 (2002).
40. Kwong,K.Y. *et al.* Expression of transforming growth factor beta (TGF-beta1) in human epithelial alveolar cells: a pro-inflammatory mediator independent pathway. *Life Sci.* **74**, 2941-2957 (2004).
41. Boyarsky,G., Hanssen,C., & Clyne,L.A. Inadequacy of high K⁺/nigericin for calibrating BCECF. I. Estimating steady-state intracellular pH. *Am. J Physiol* **271**, C1131-C1145 (1996).
42. Scaduto,R.C., Jr. & Grotyohann,L.W. Measurement of mitochondrial membrane potential using fluorescent rhodamine derivatives. *Biophys. J* **76**, 469-477 (1999).
43. Kiefmann,R. *et al.* Role of poly(ADP-ribose) synthetase in pulmonary leukocyte recruitment. *Am. J. Physiol Lung Cell Mol. Physiol* **285**, L996-L1005 (2003).
44. Kuebler,W.M. *et al.* Role of L-selectin in leukocyte sequestration in lung capillaries in a rabbit model of endotoxemia. *Am. J. Respir. Crit Care Med.* **161**, 36-43 (2000).

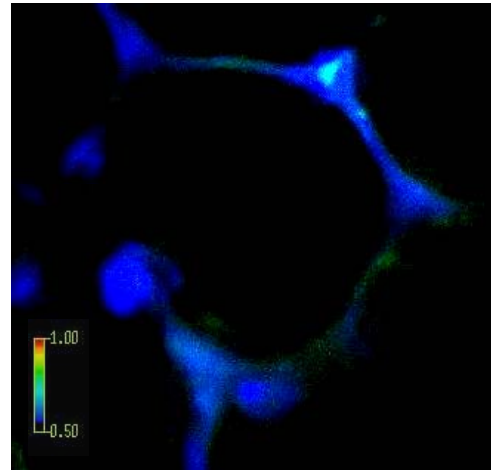
Figure 1

A

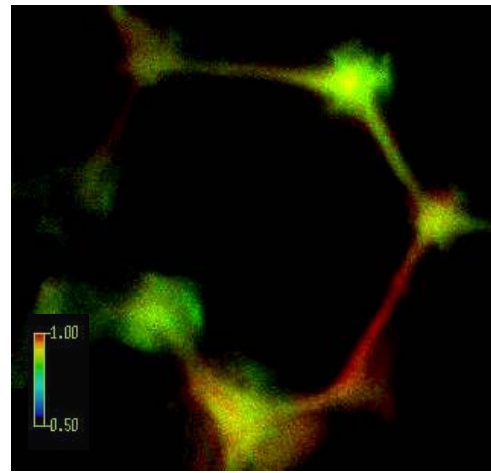
fura 2 ratio 340/380nm



5 Vol% CO₂



0 Vol% CO₂



10 Vol% CO₂

B

[CO₂]_{iA}: 5 Vol% 0 Vol% 5 Vol% 10 Vol% 5 Vol%

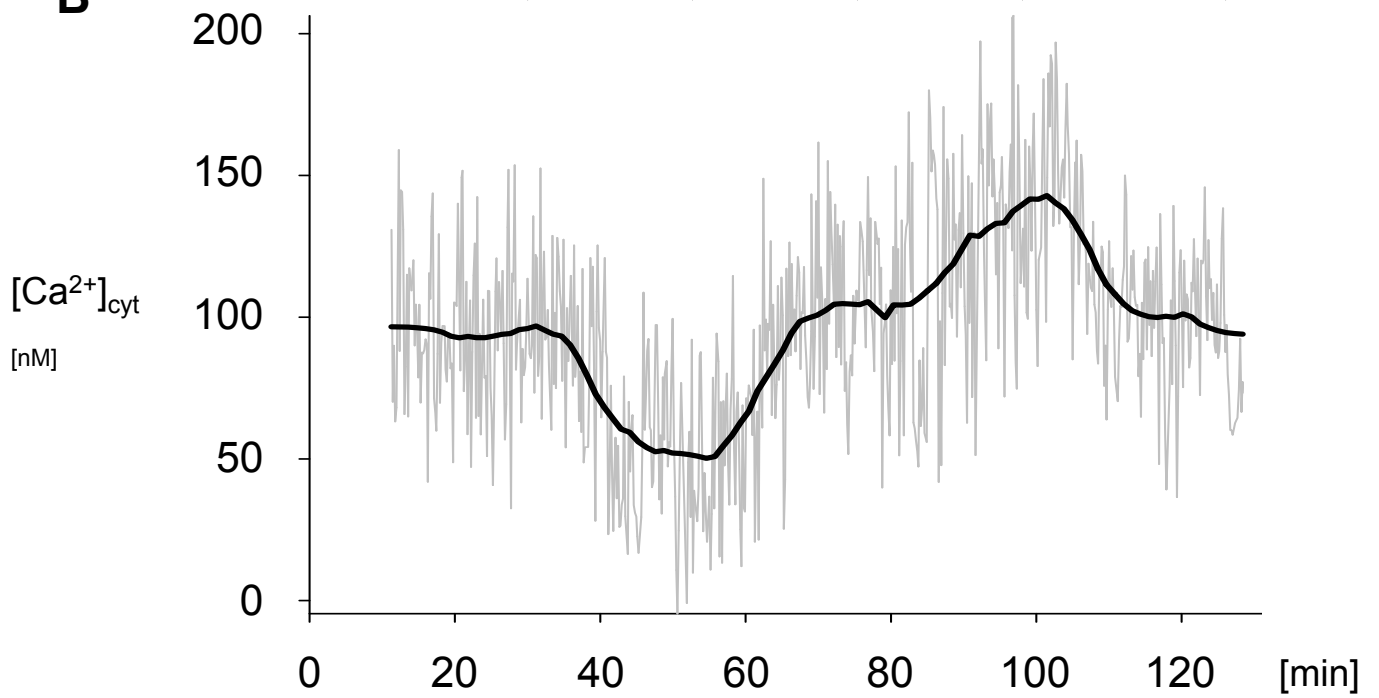
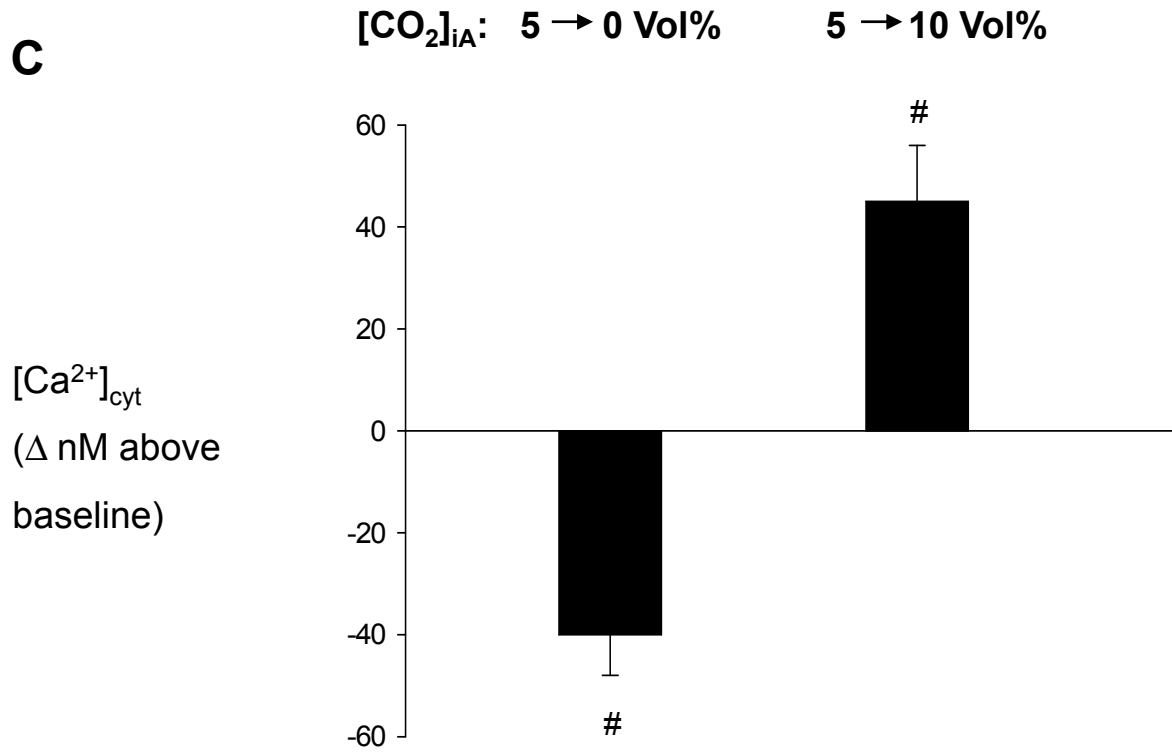


Figure 1

C



D

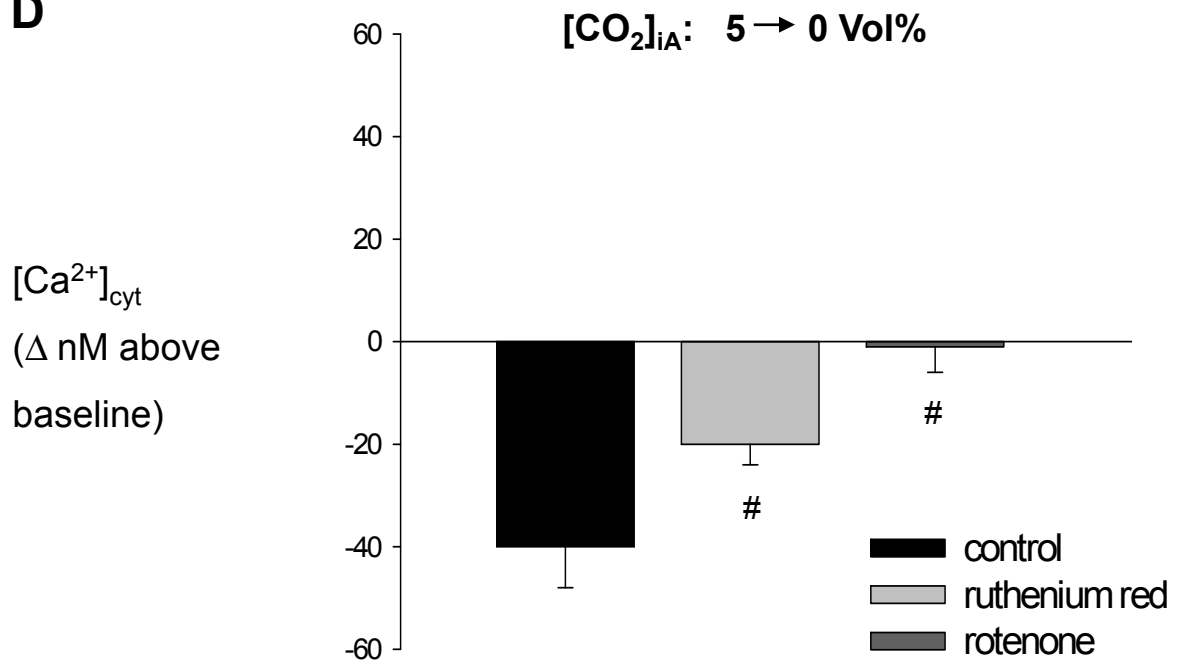
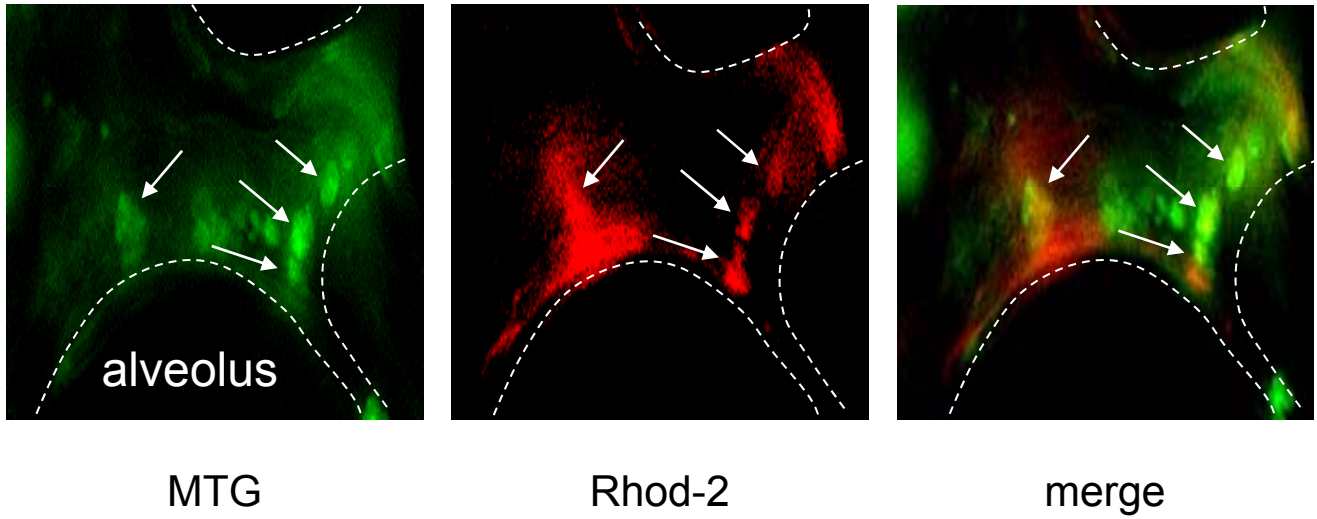


Figure 2

A



B

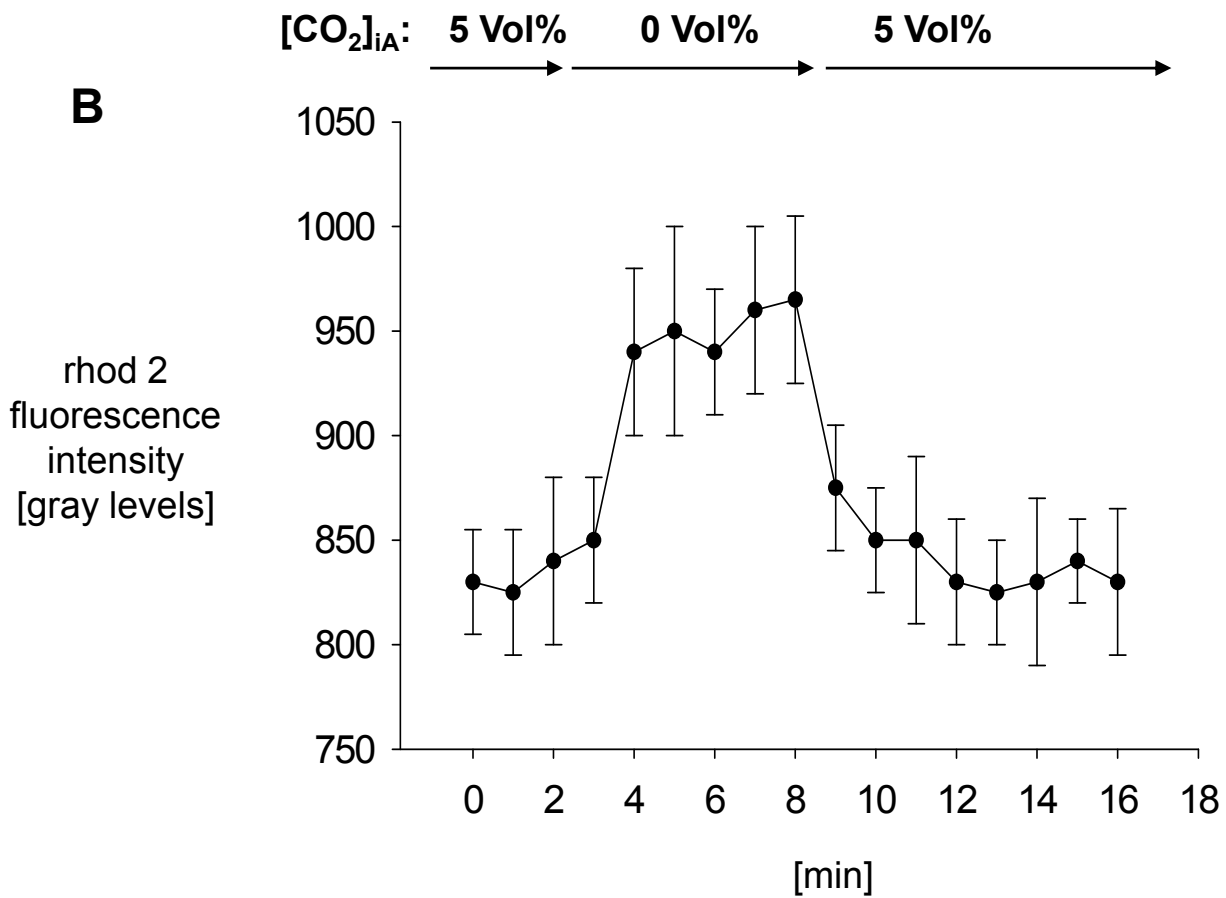


Figure 3

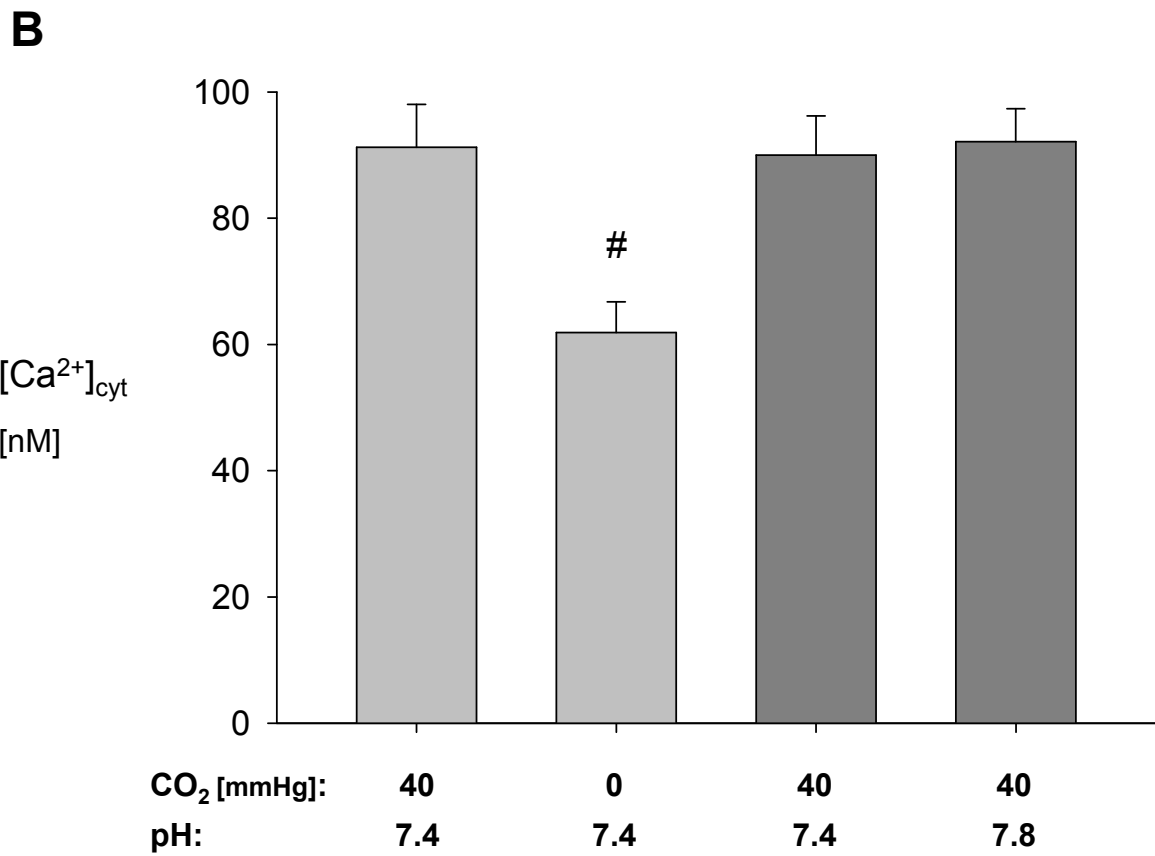
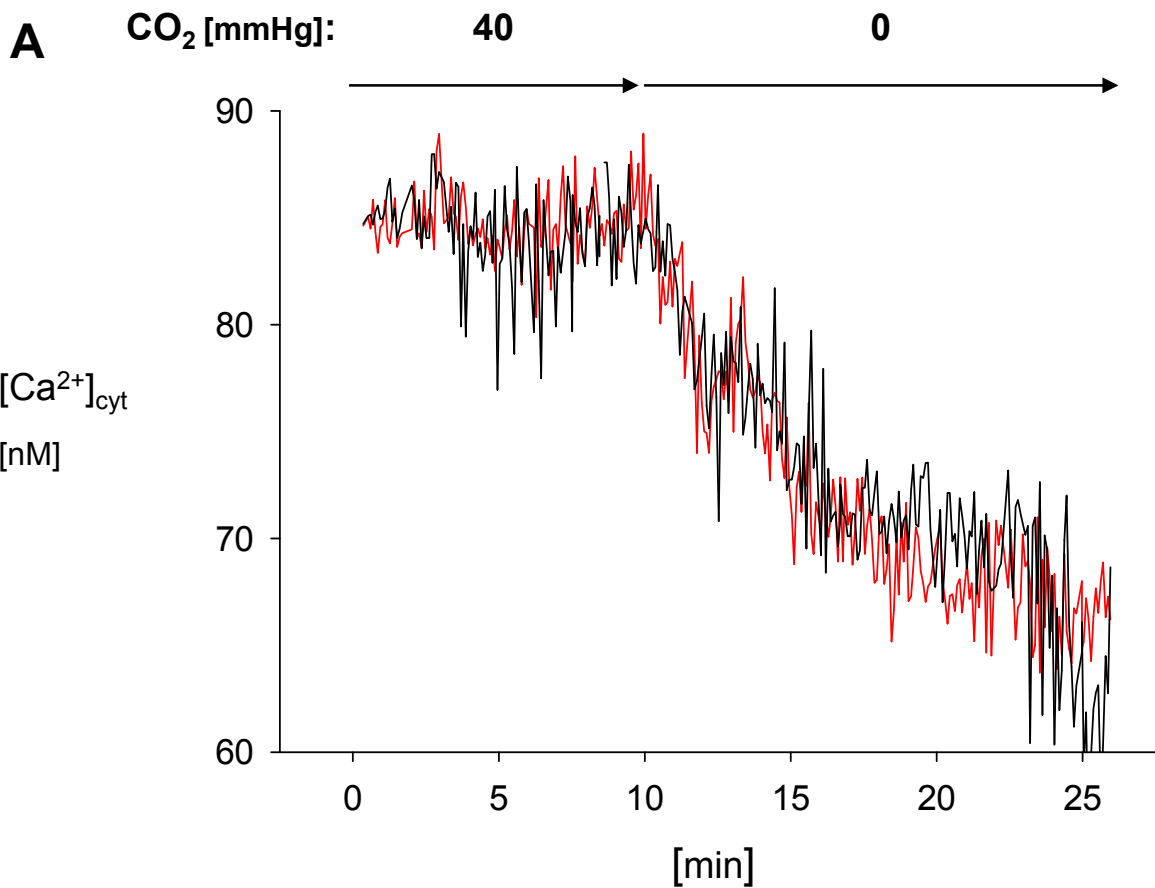
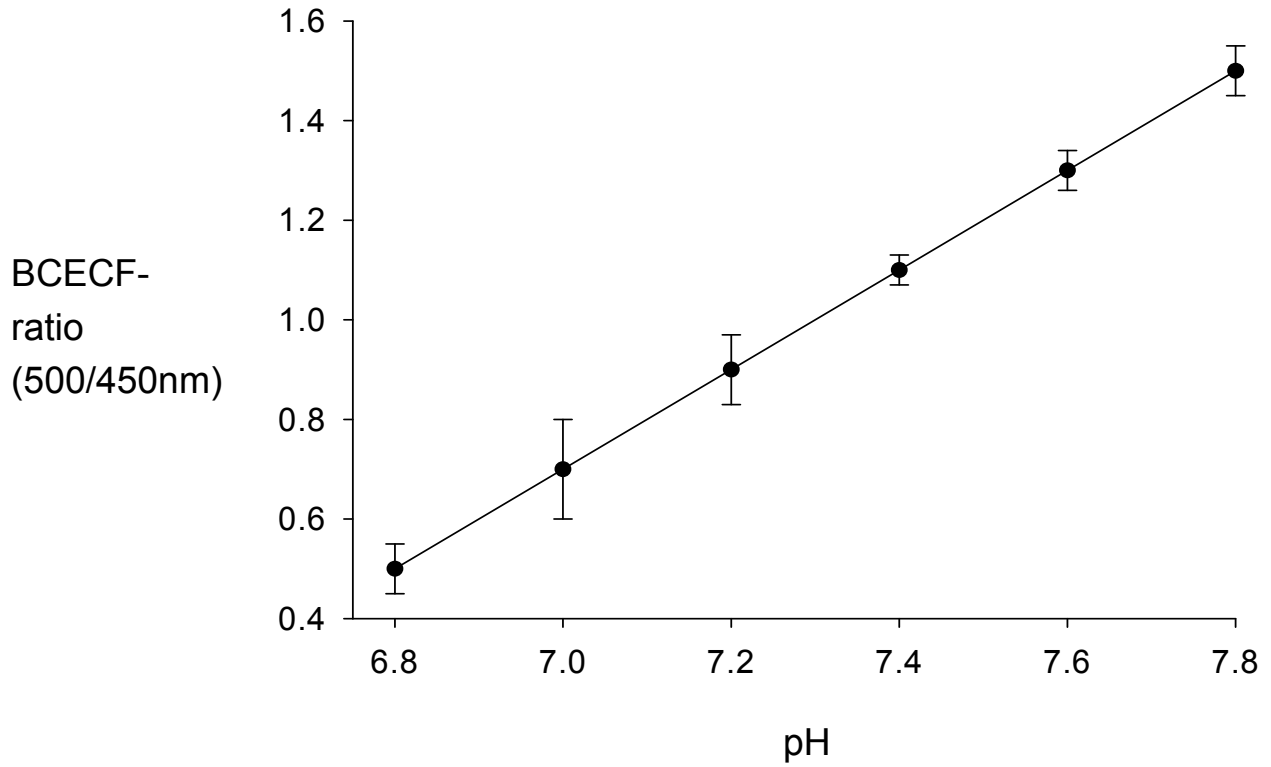


Figure 3

C



D

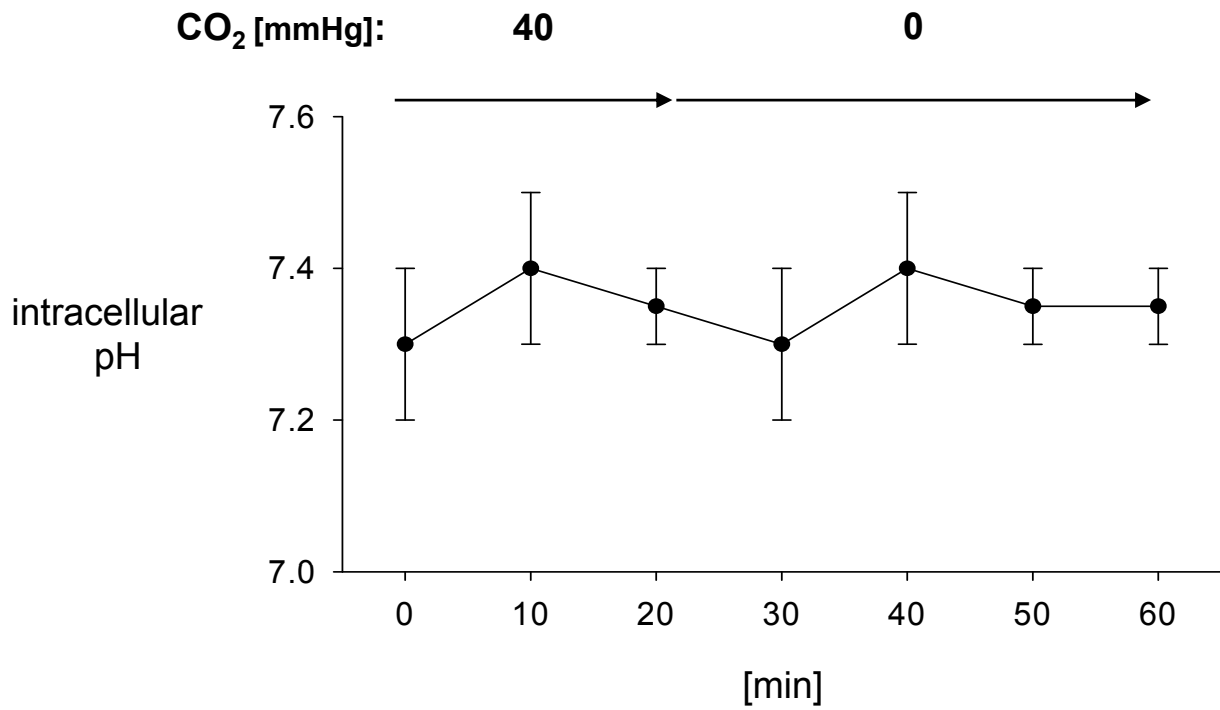


Figure 4

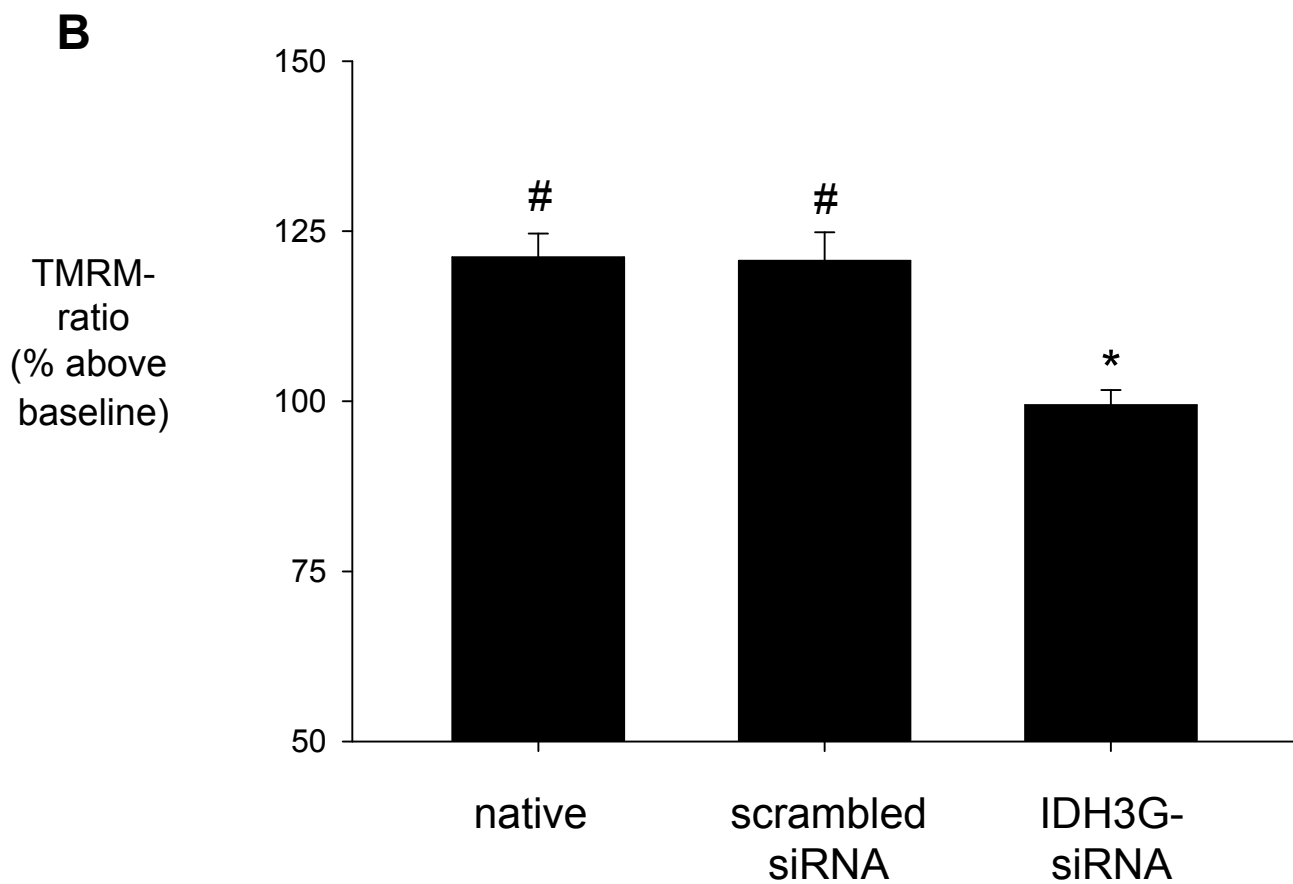
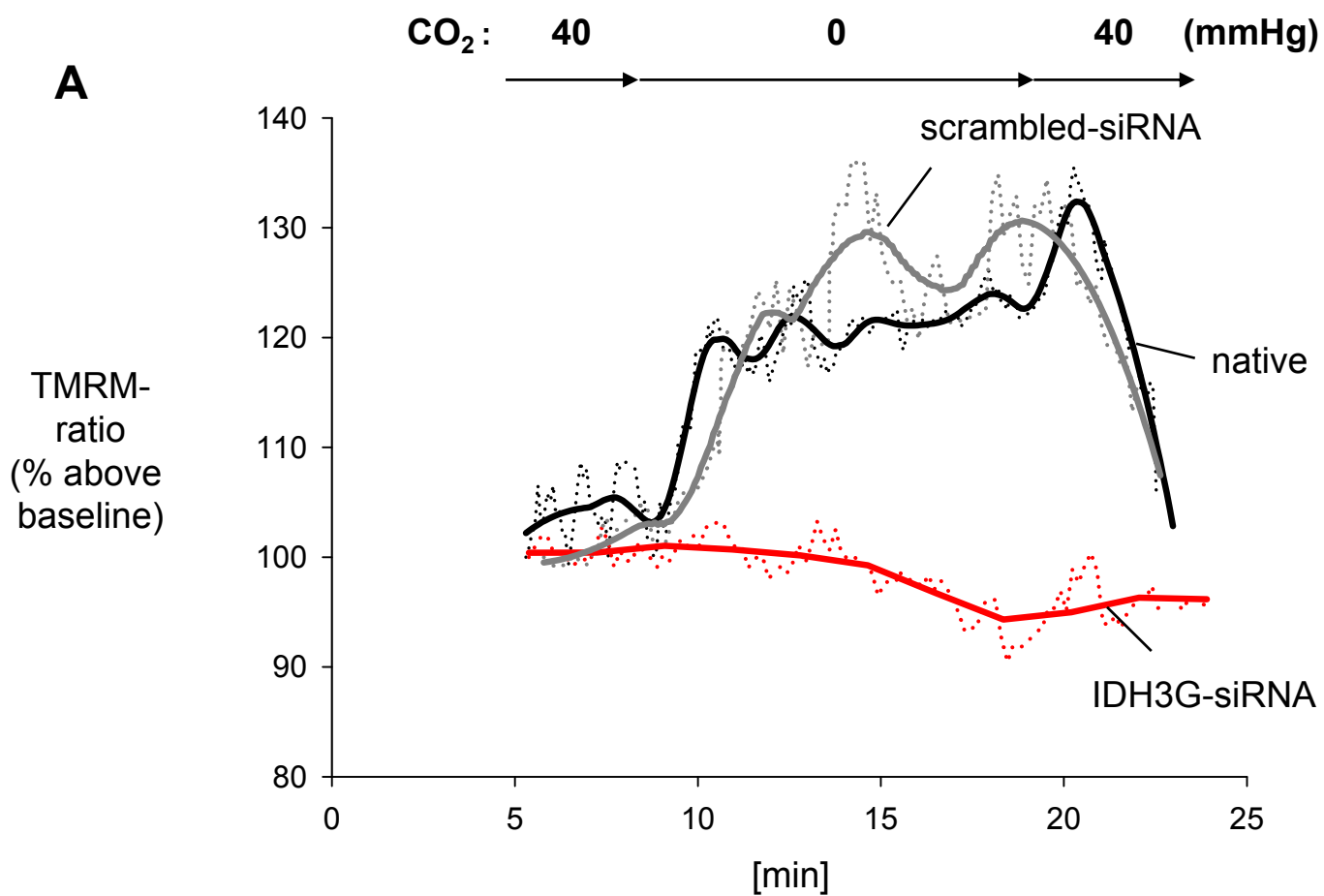


Figure 4

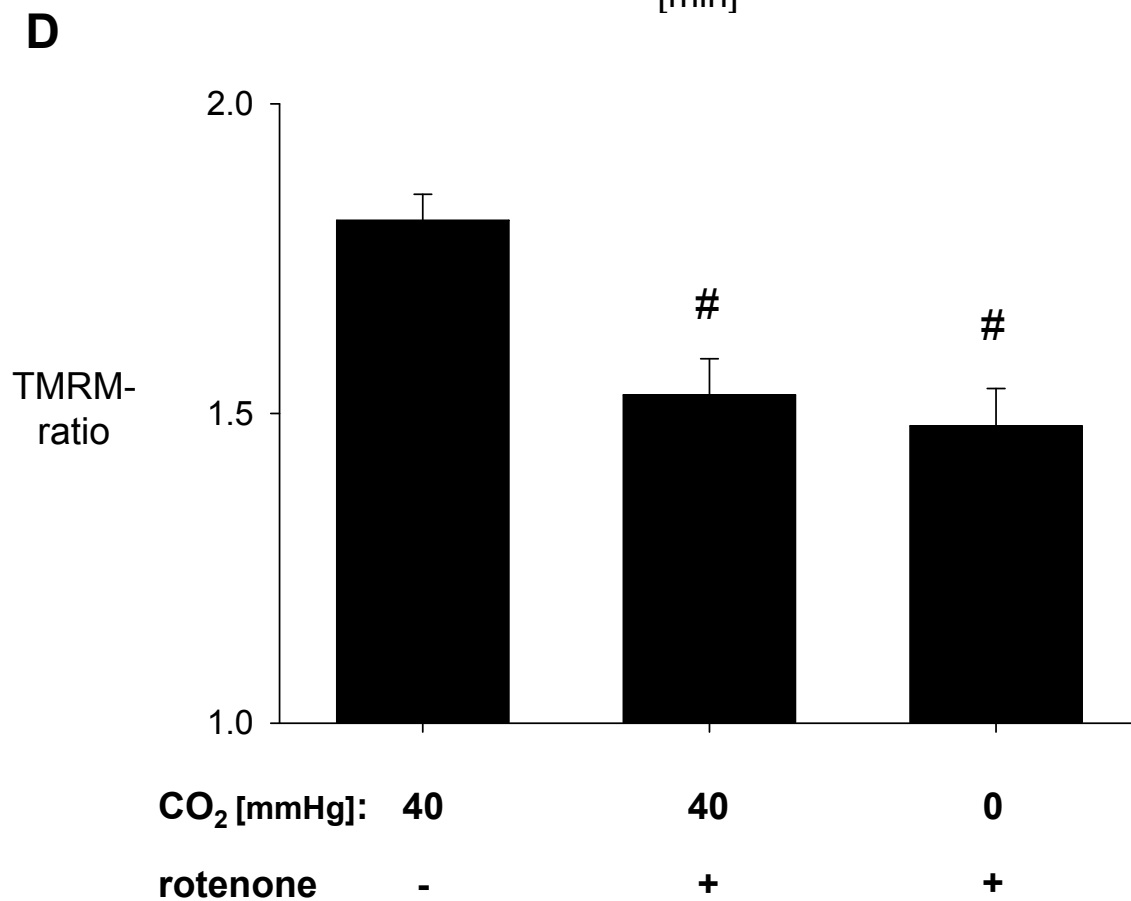
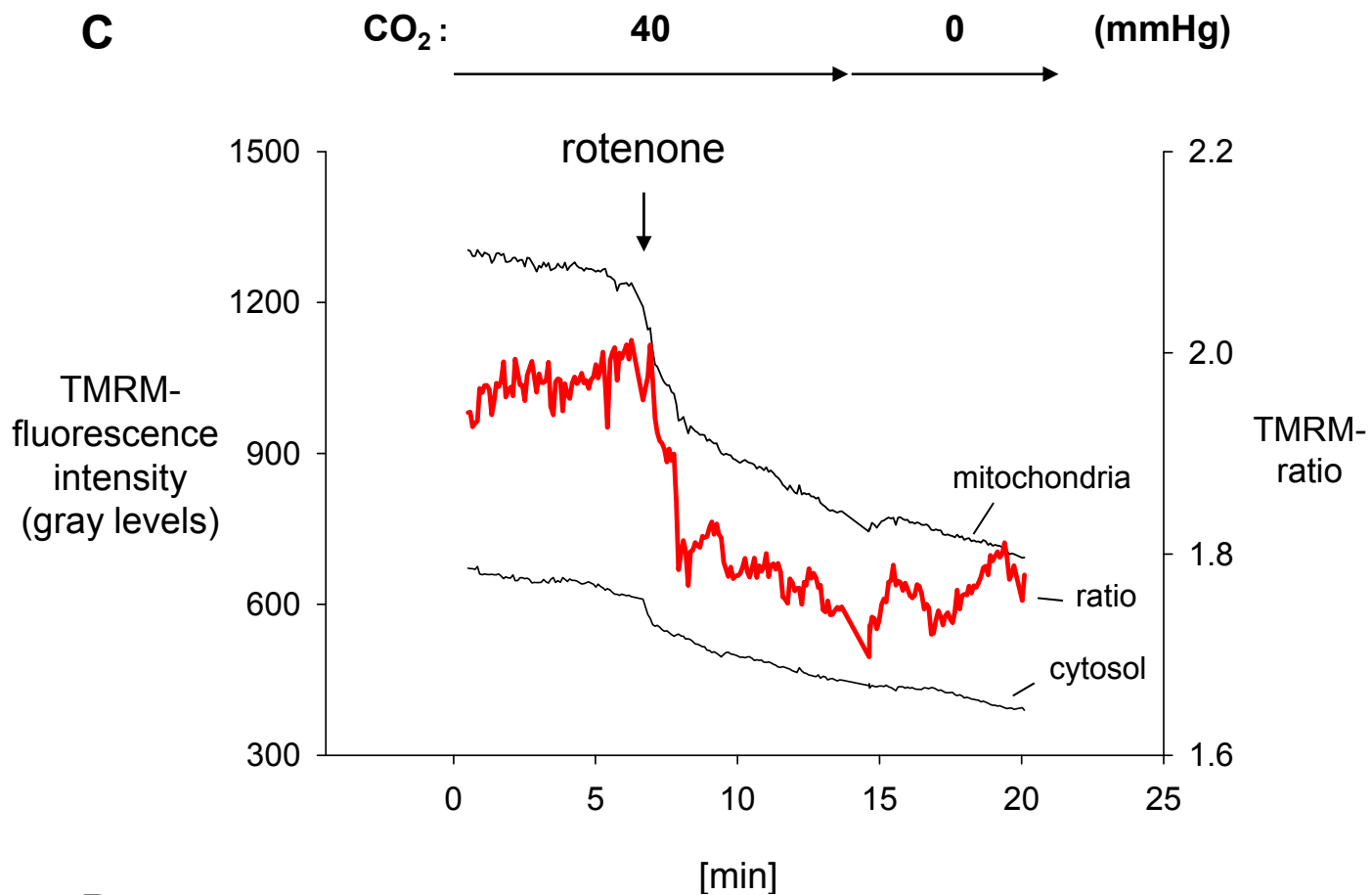
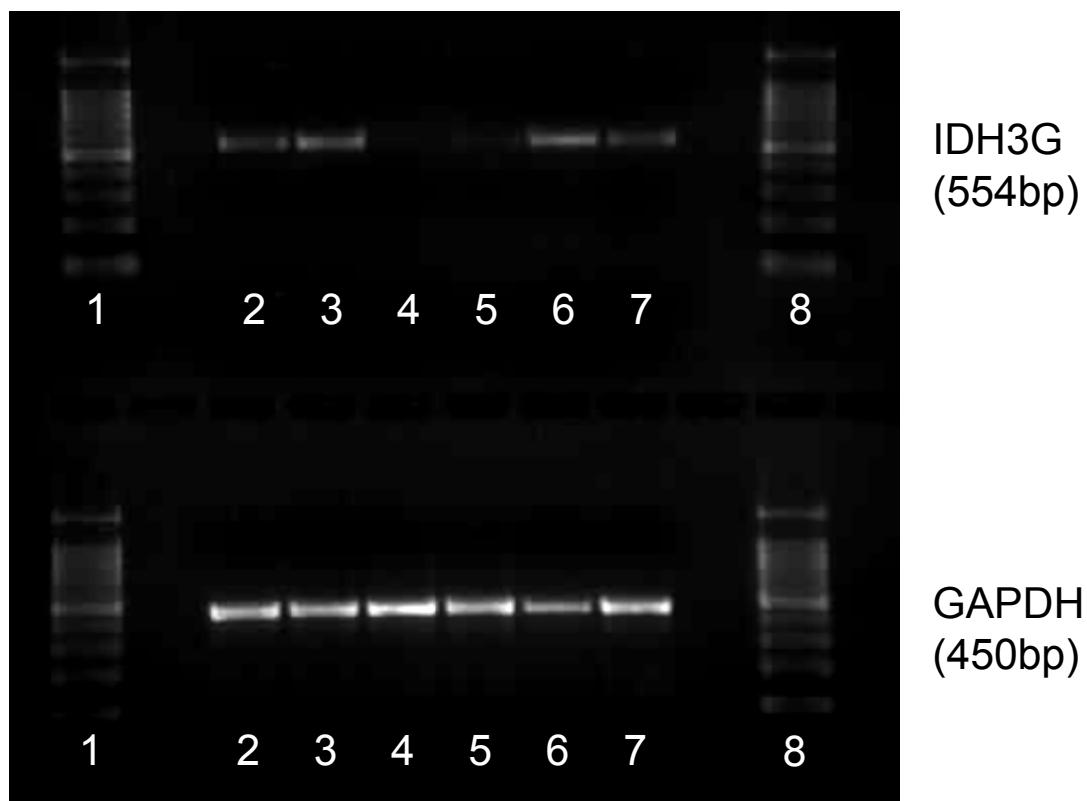


Figure 4

E



F

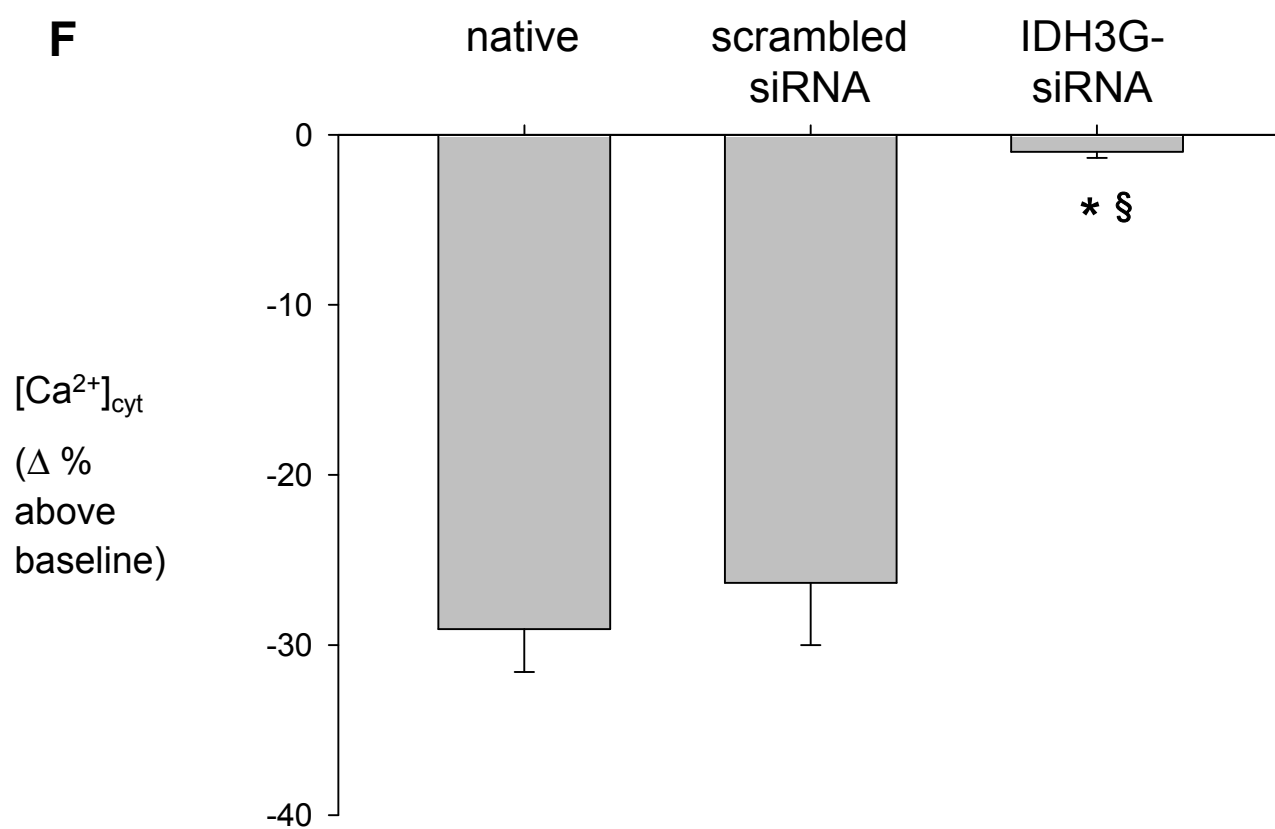


Figure 4

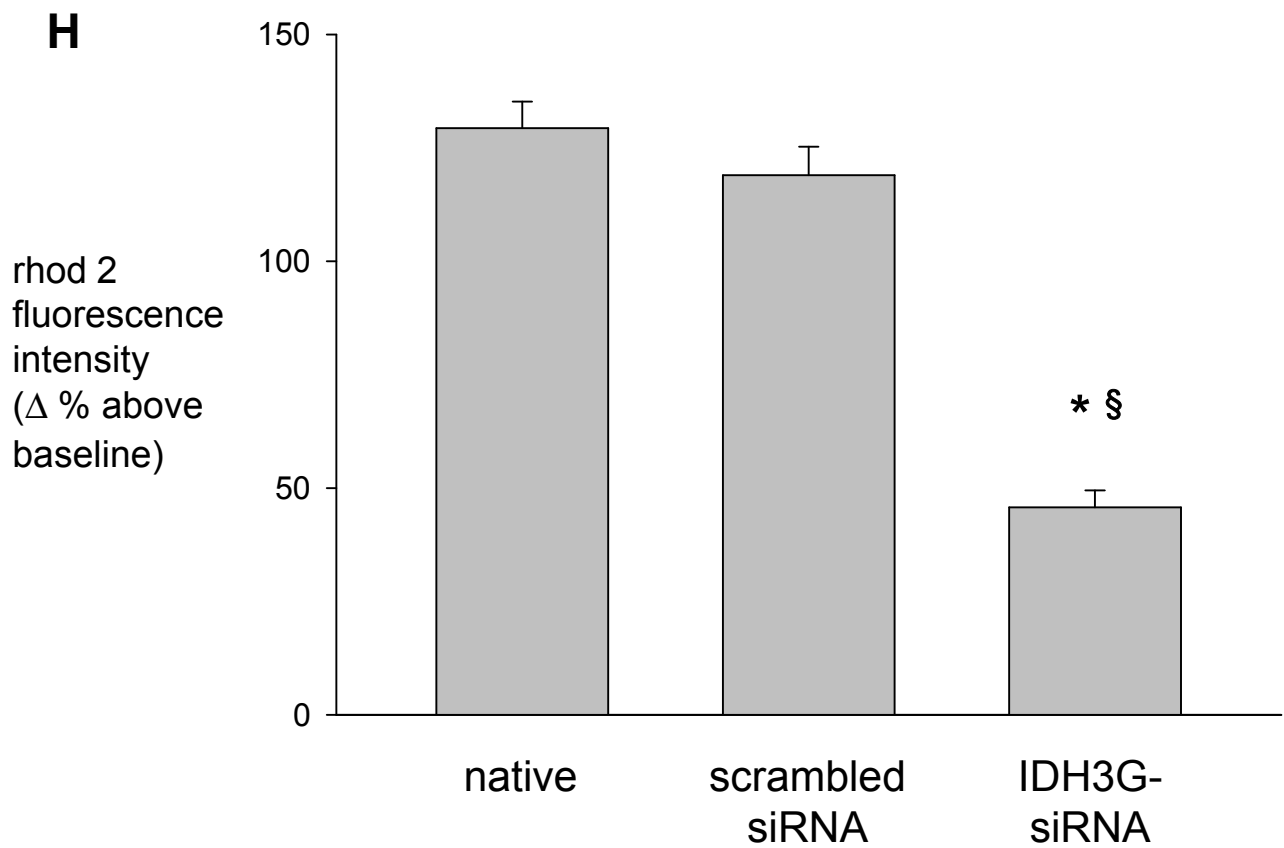
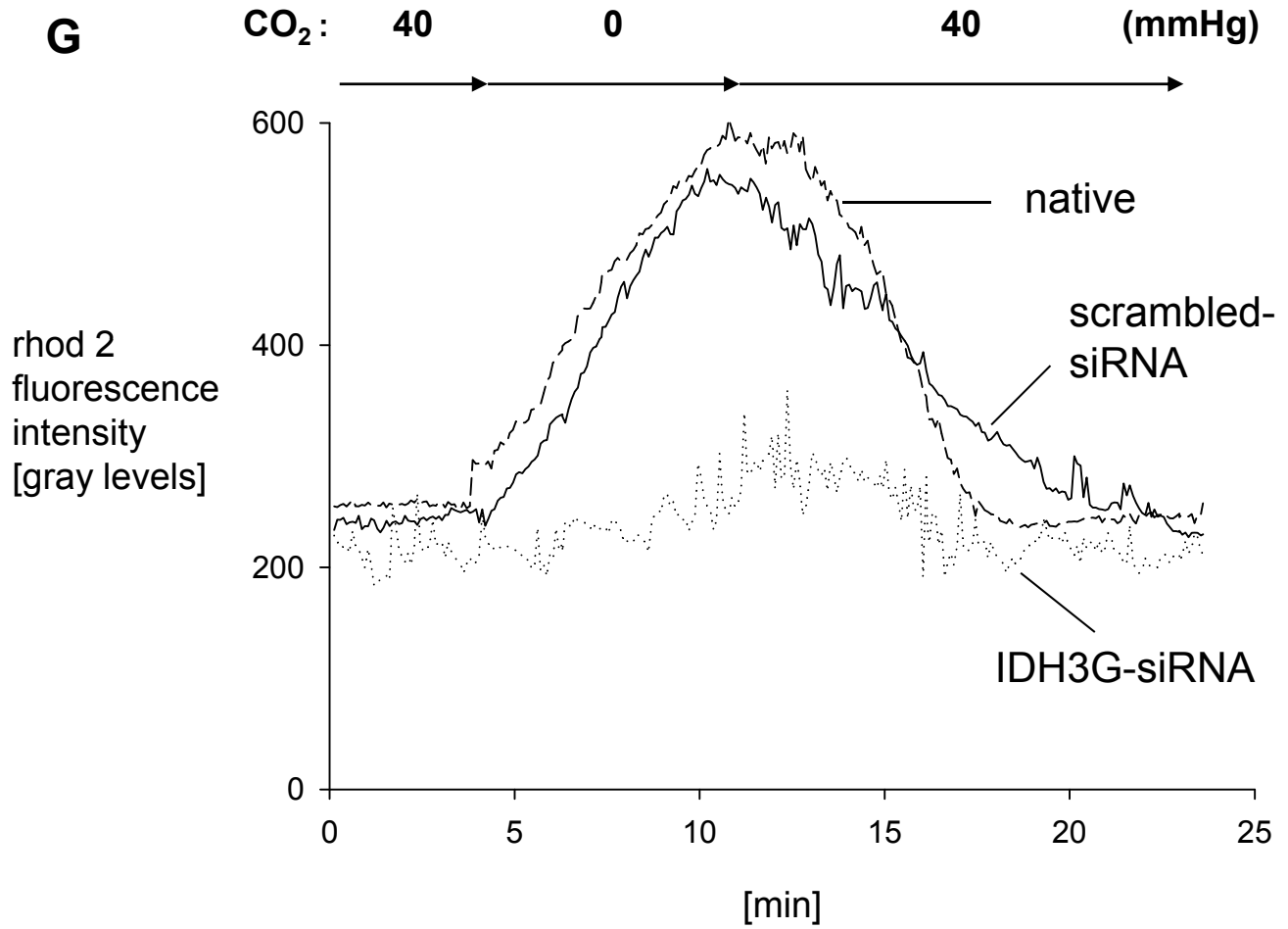


Figure 4

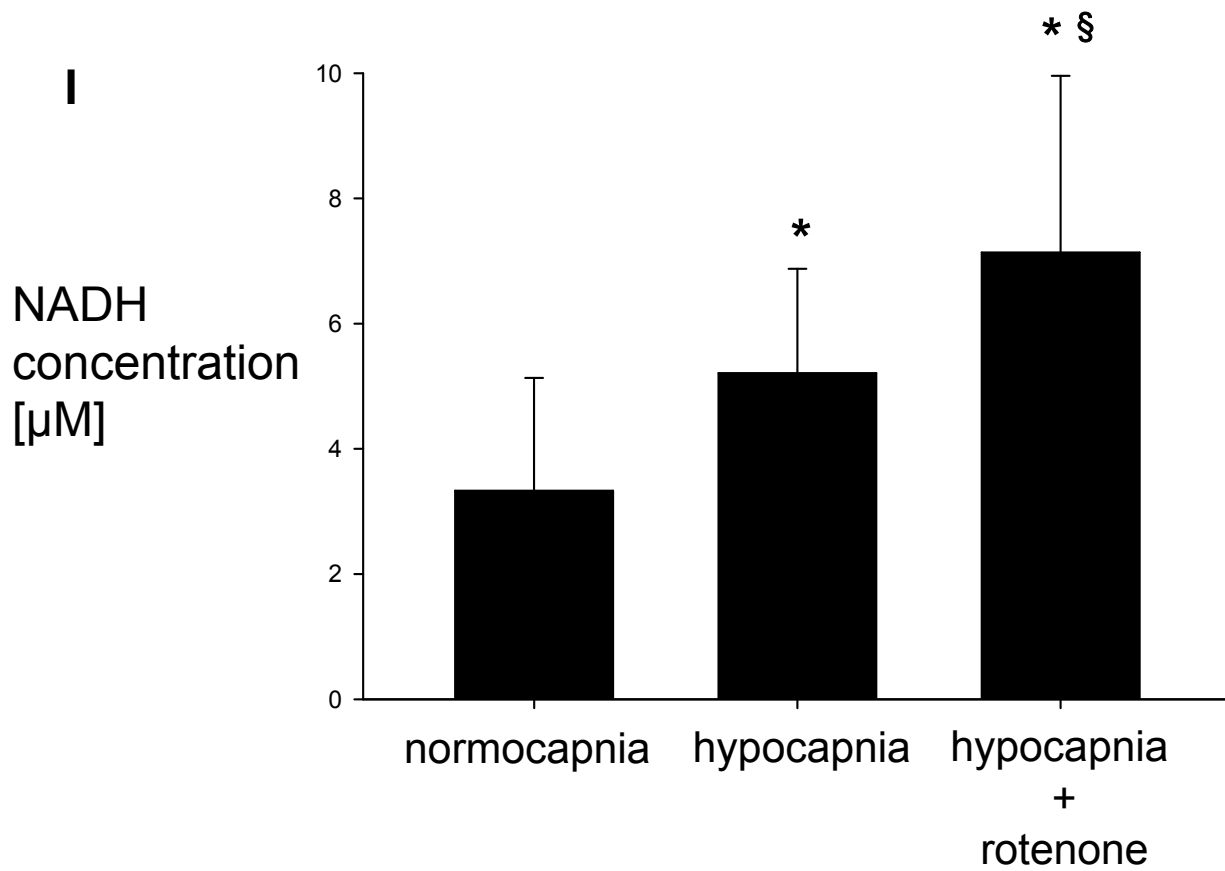


Figure 4

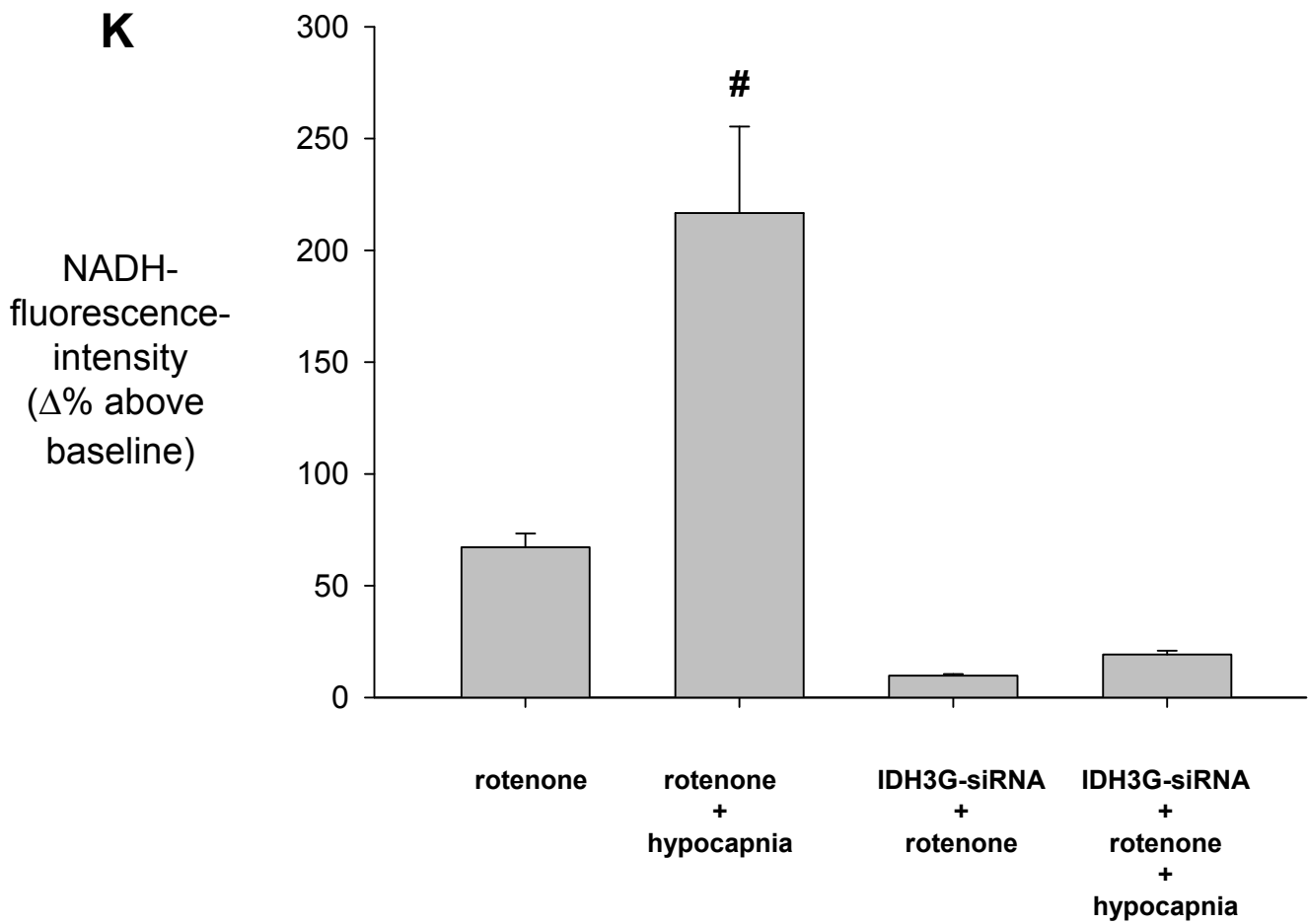
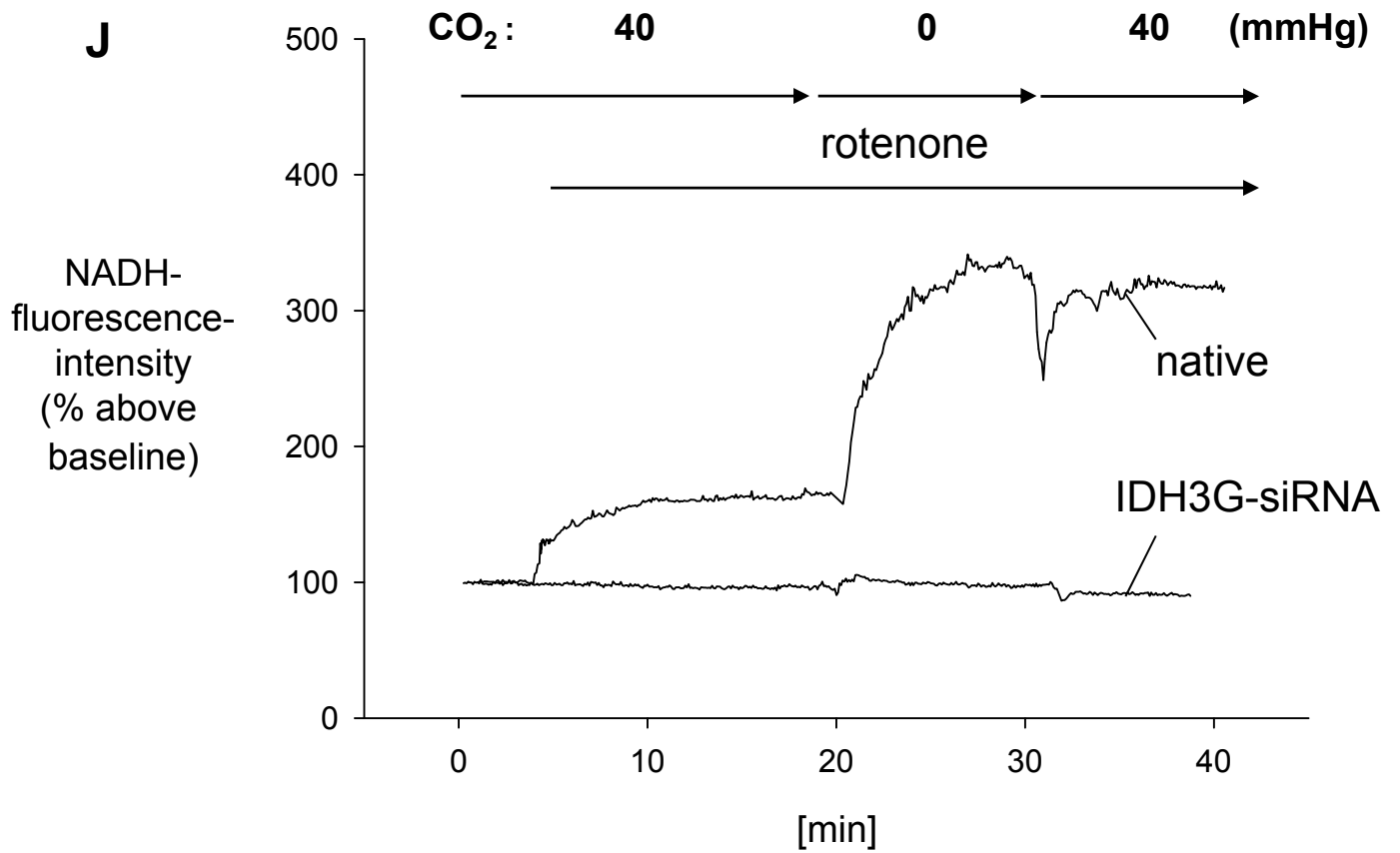
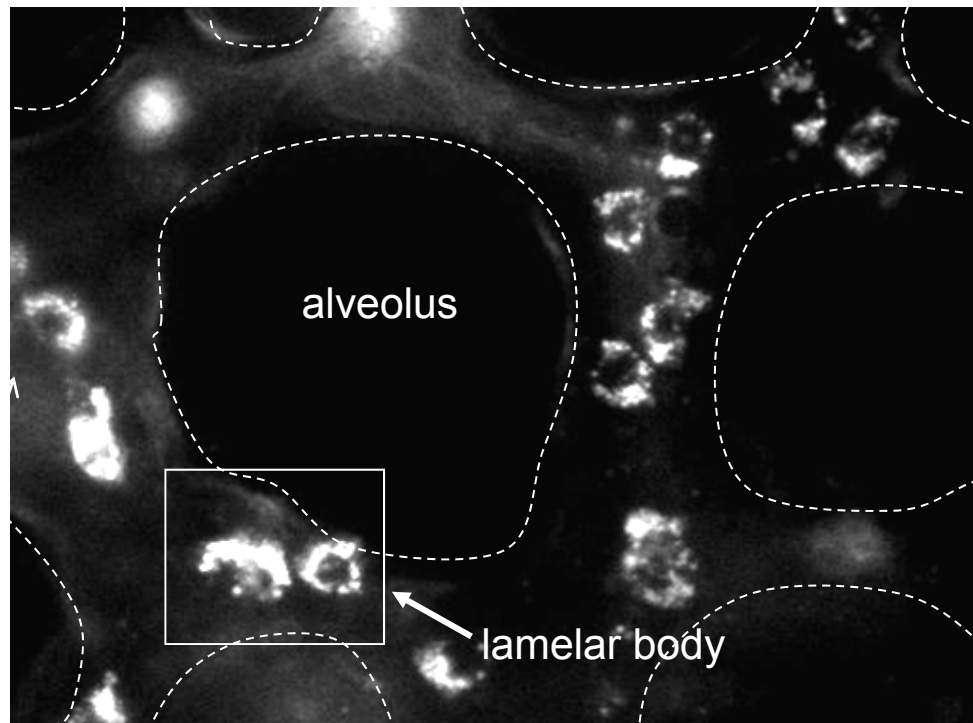


Figure 5

A



B

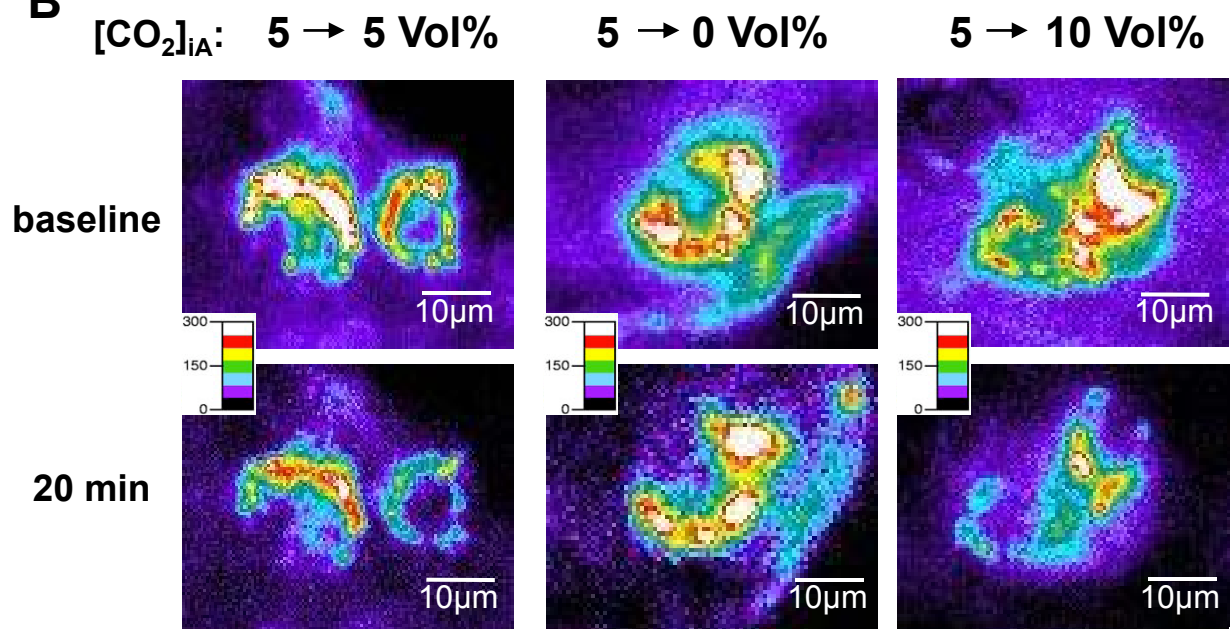


Figure 5

C

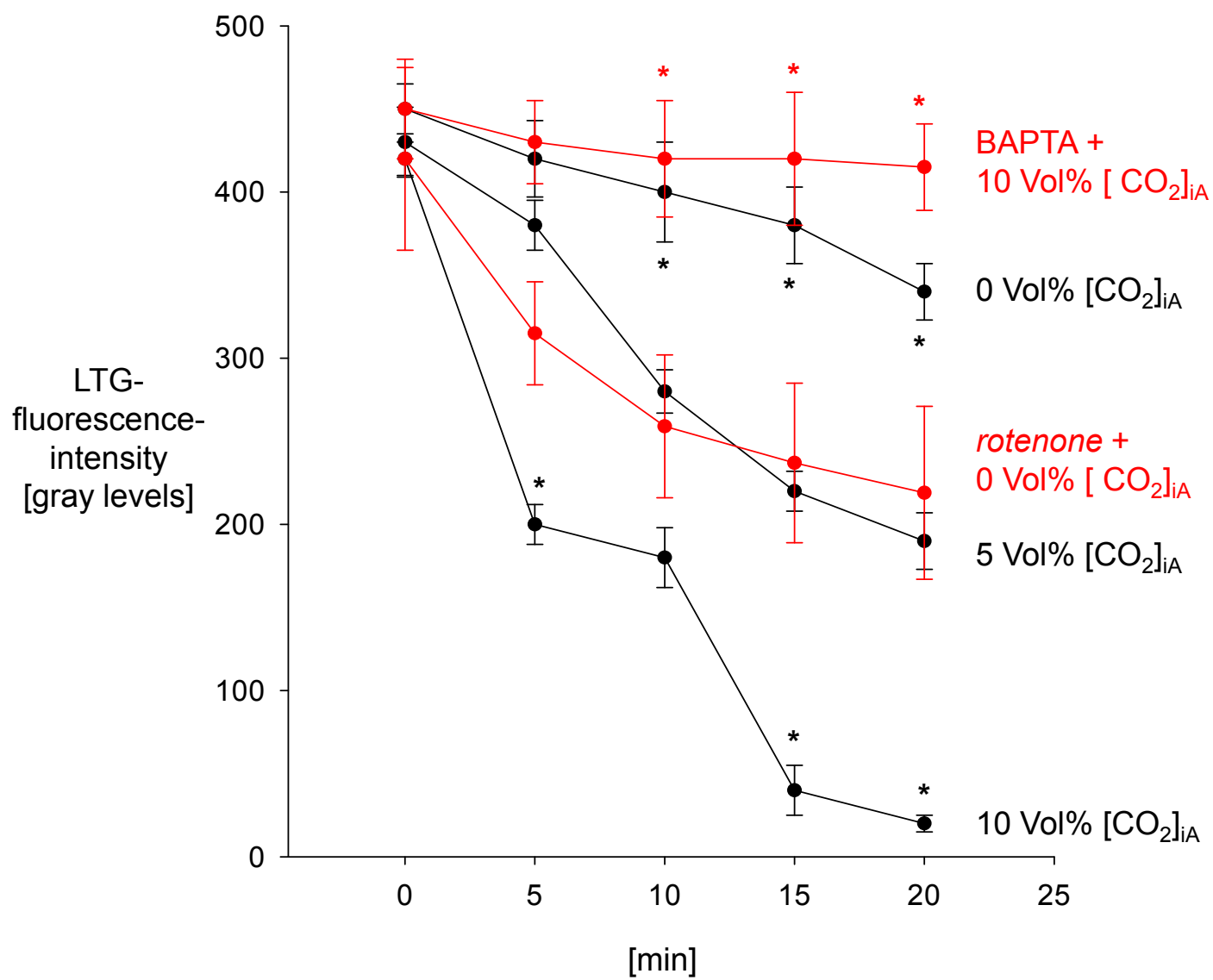
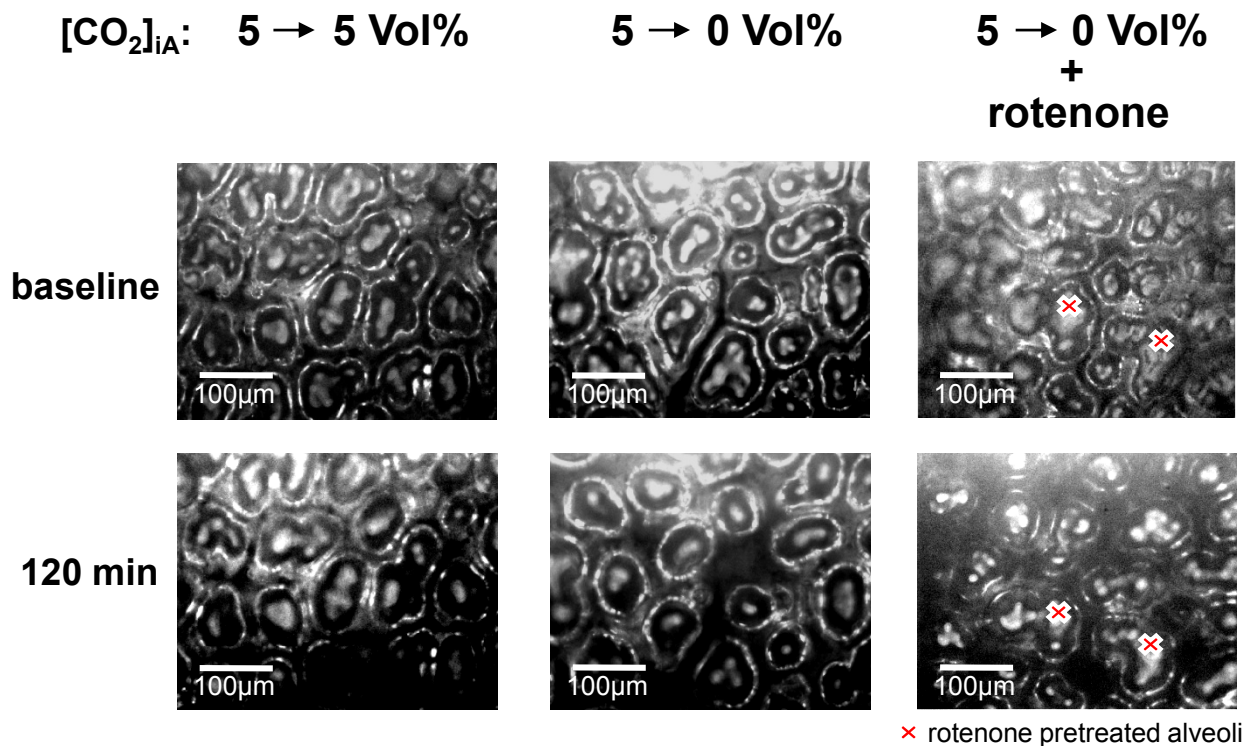


Figure 5

D



E

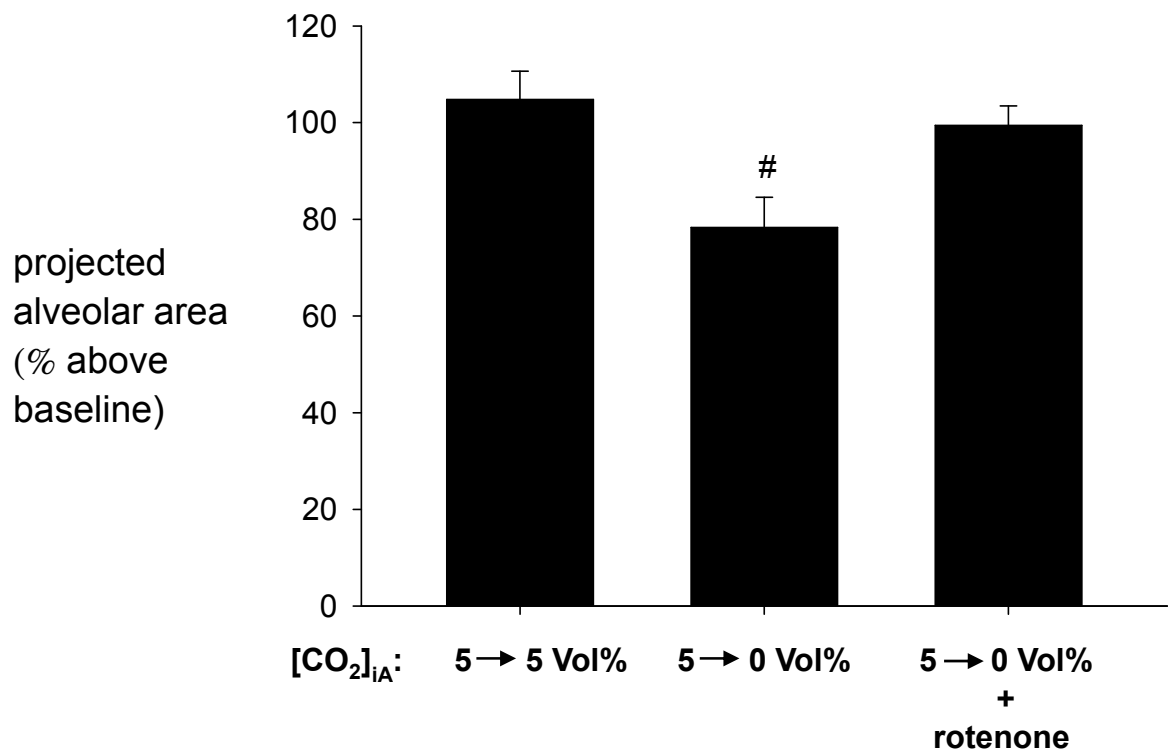


Figure 6

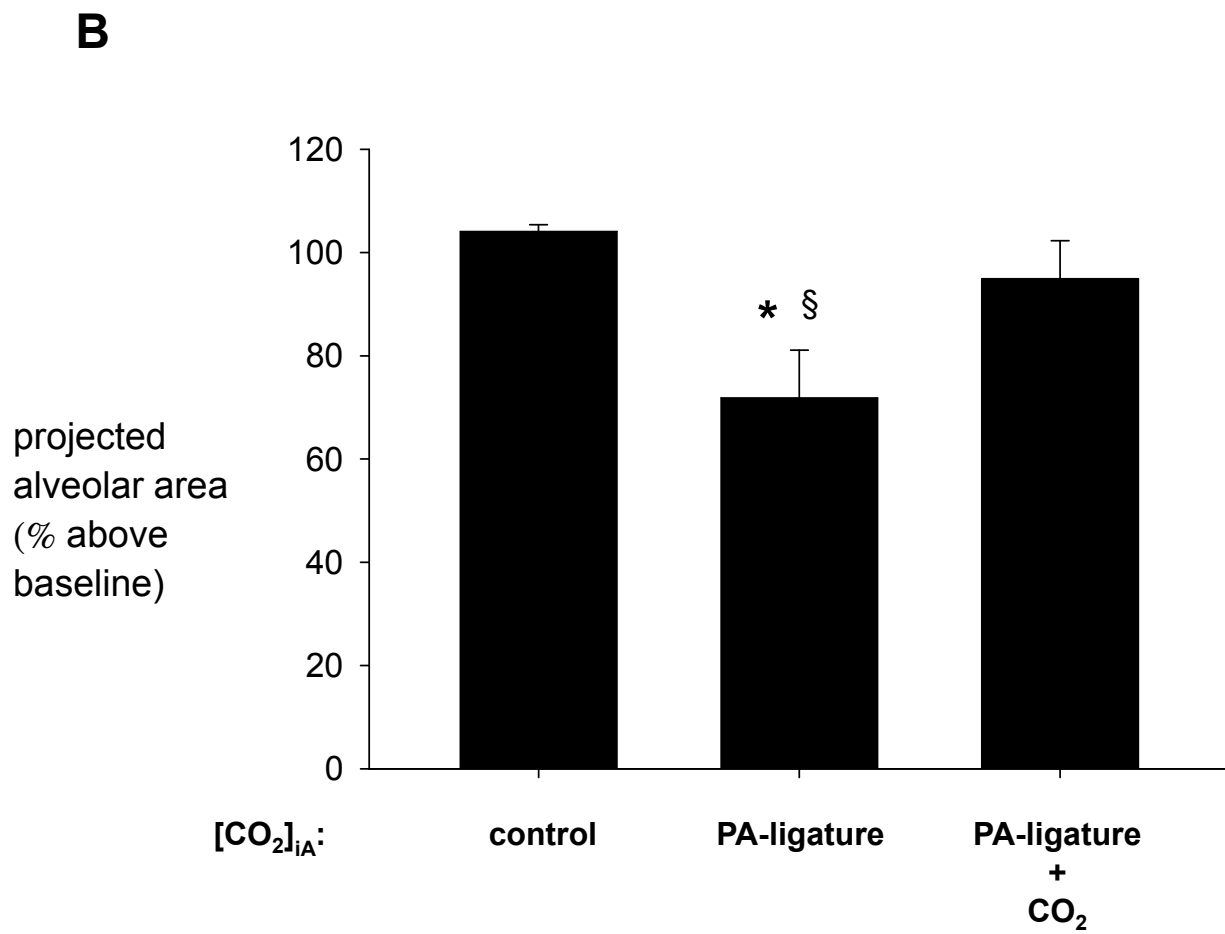
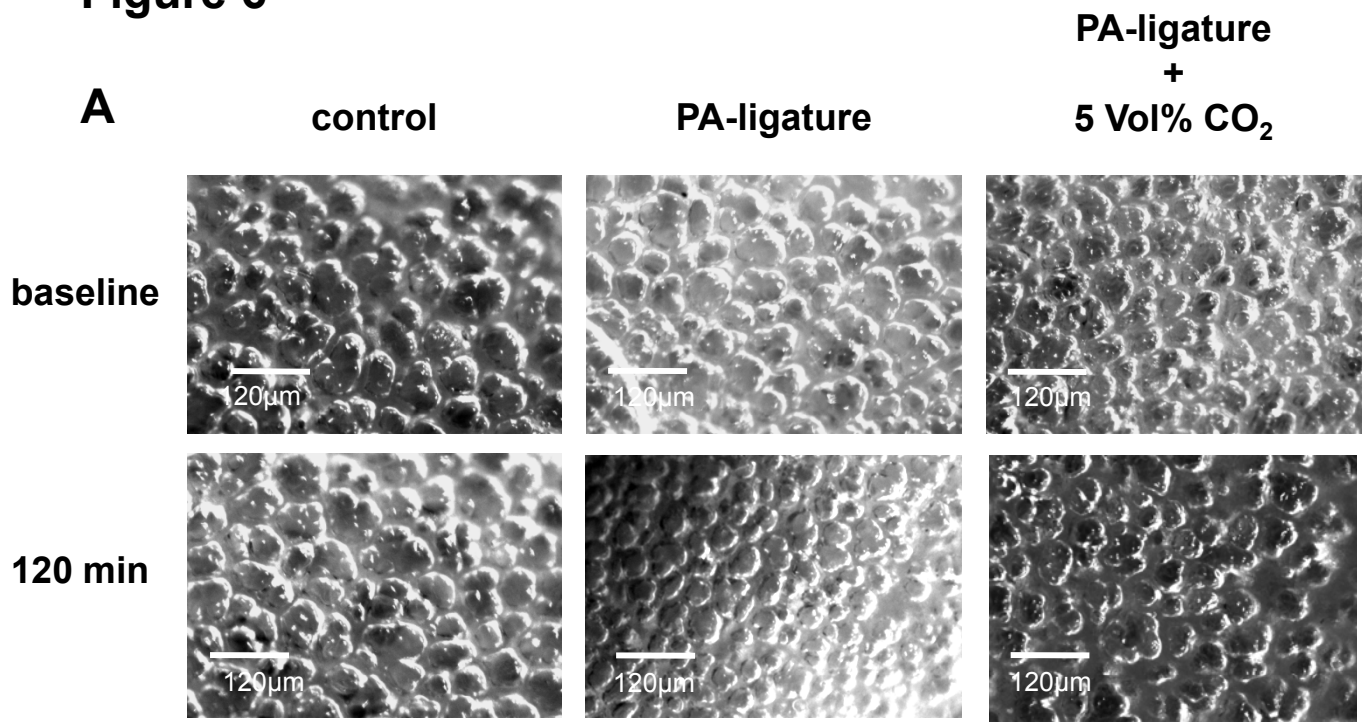
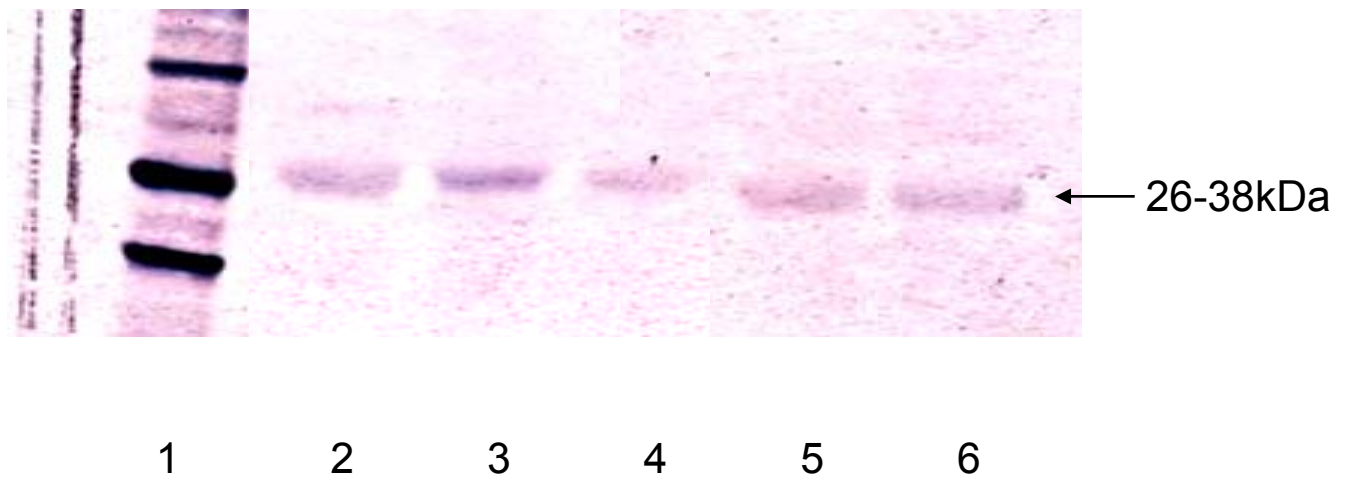


Figure 6

C



D

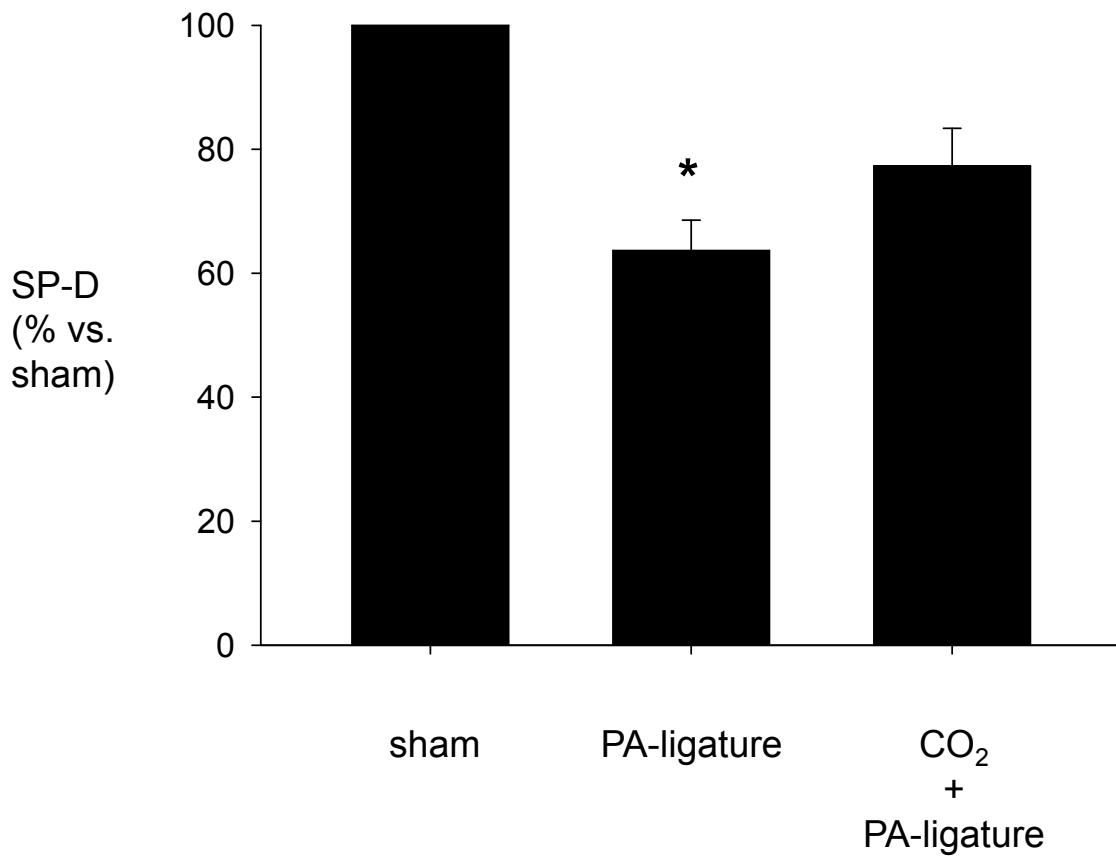


Figure 6

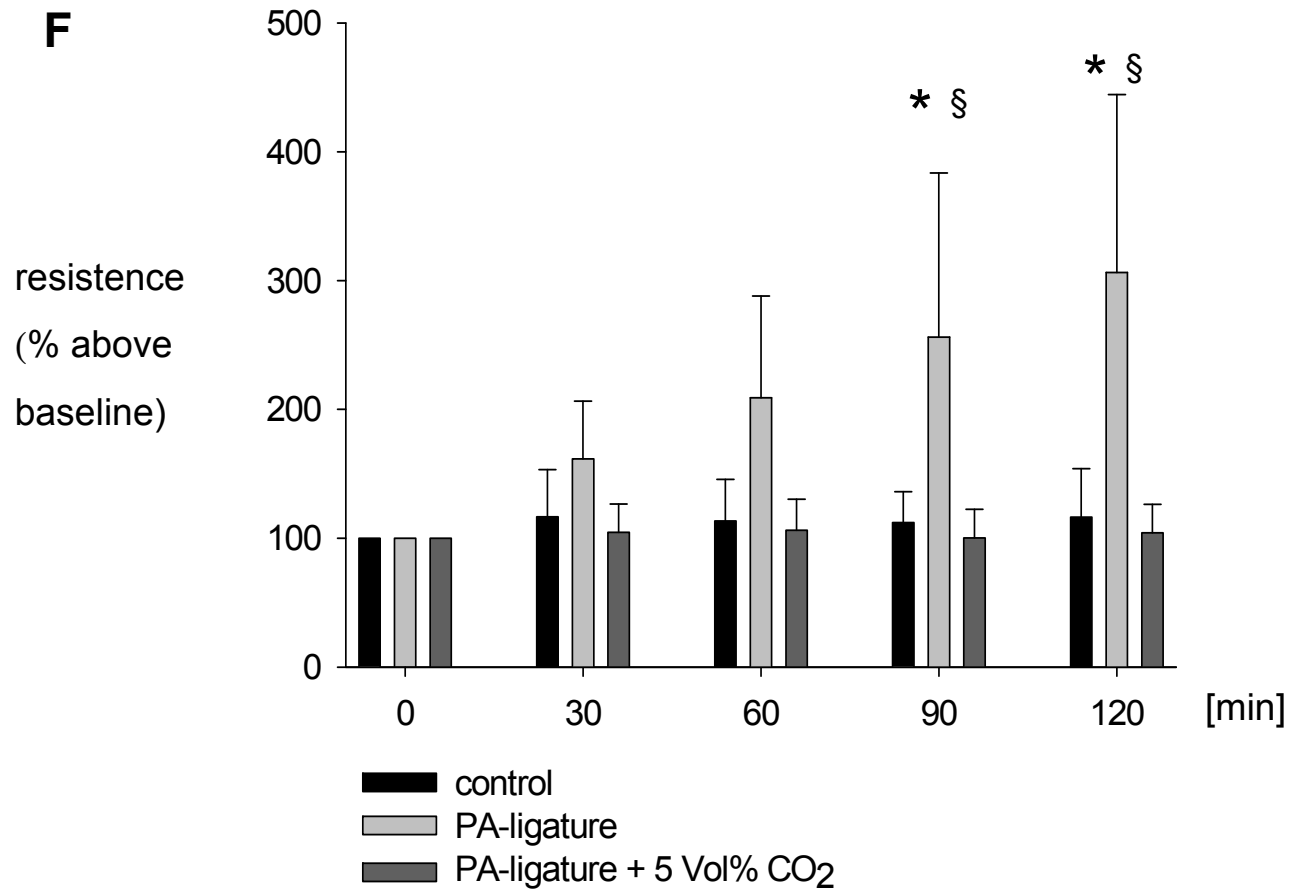
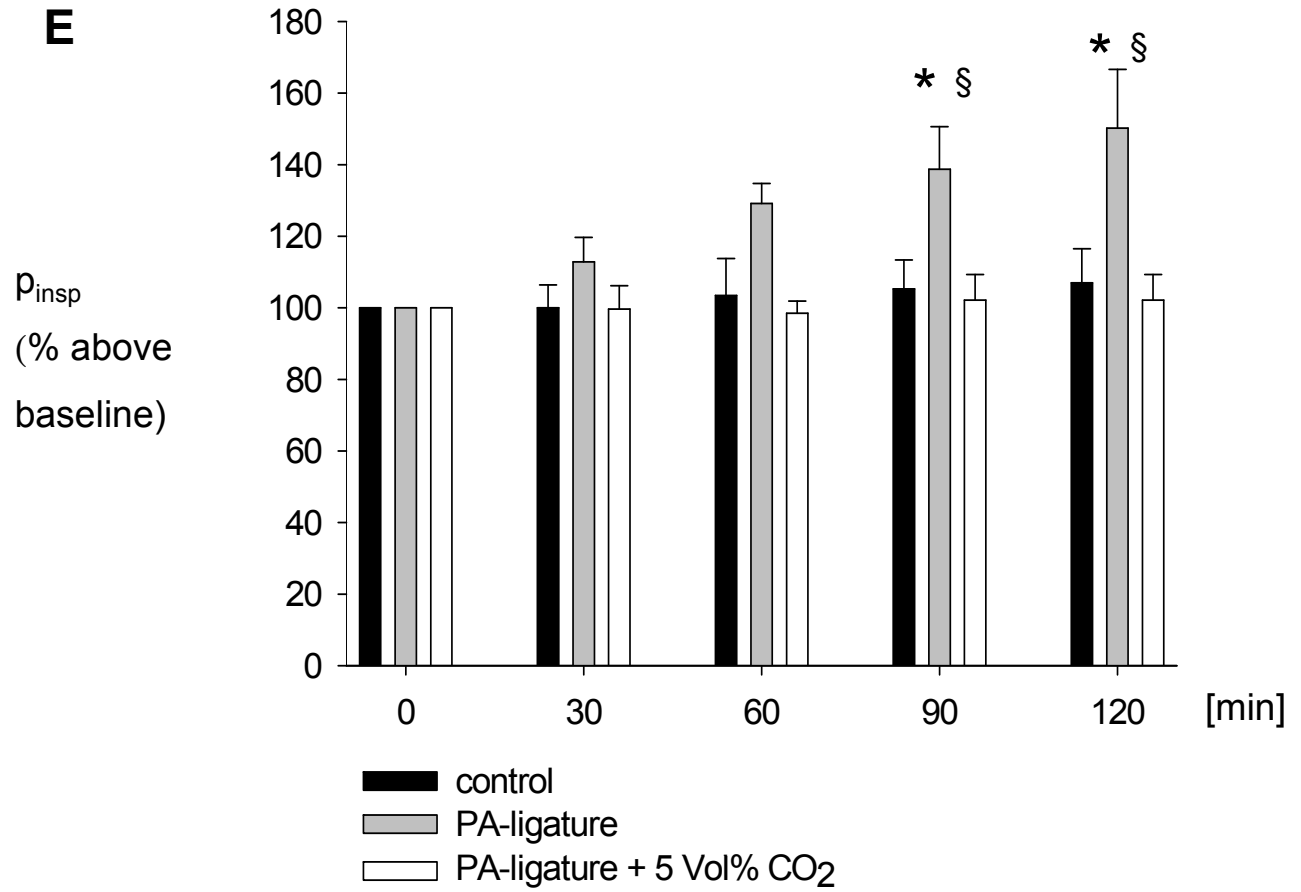


Figure 6

G

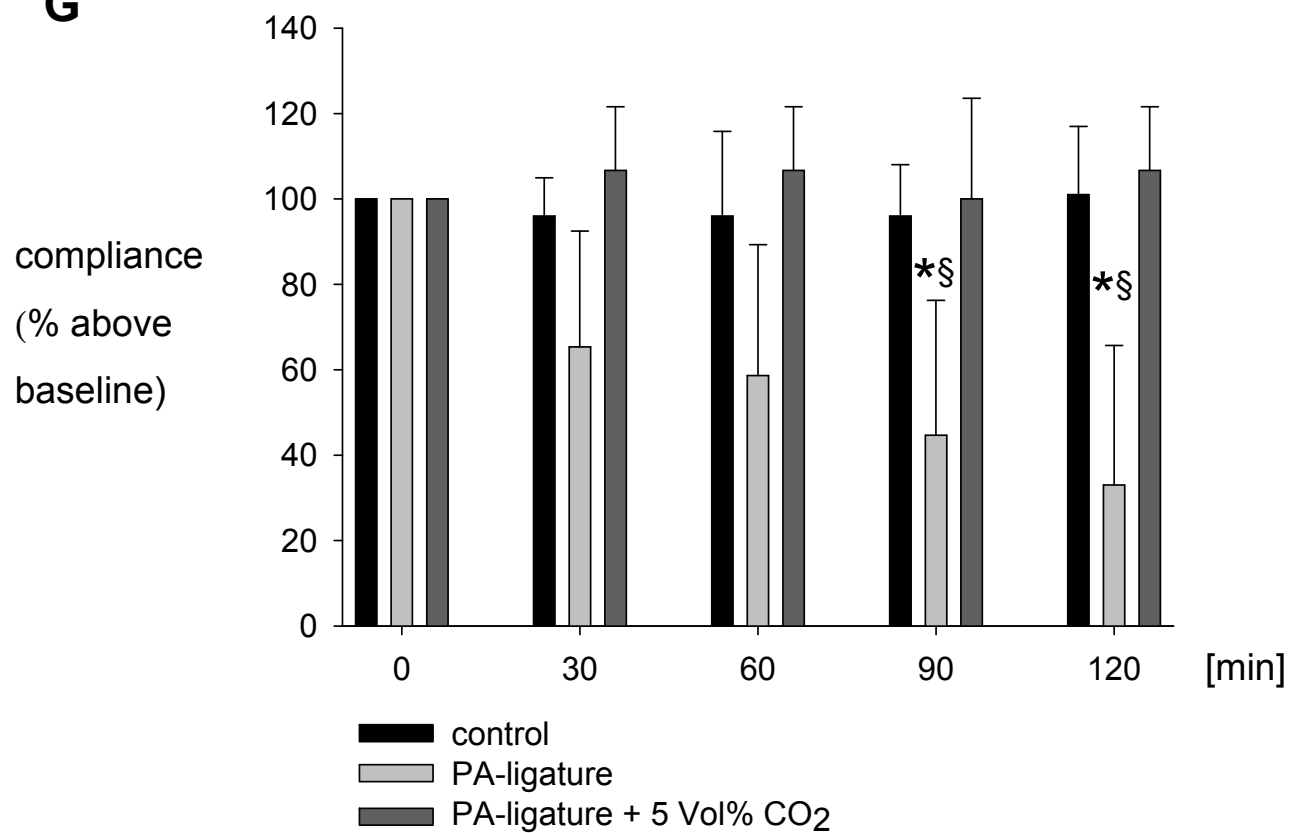
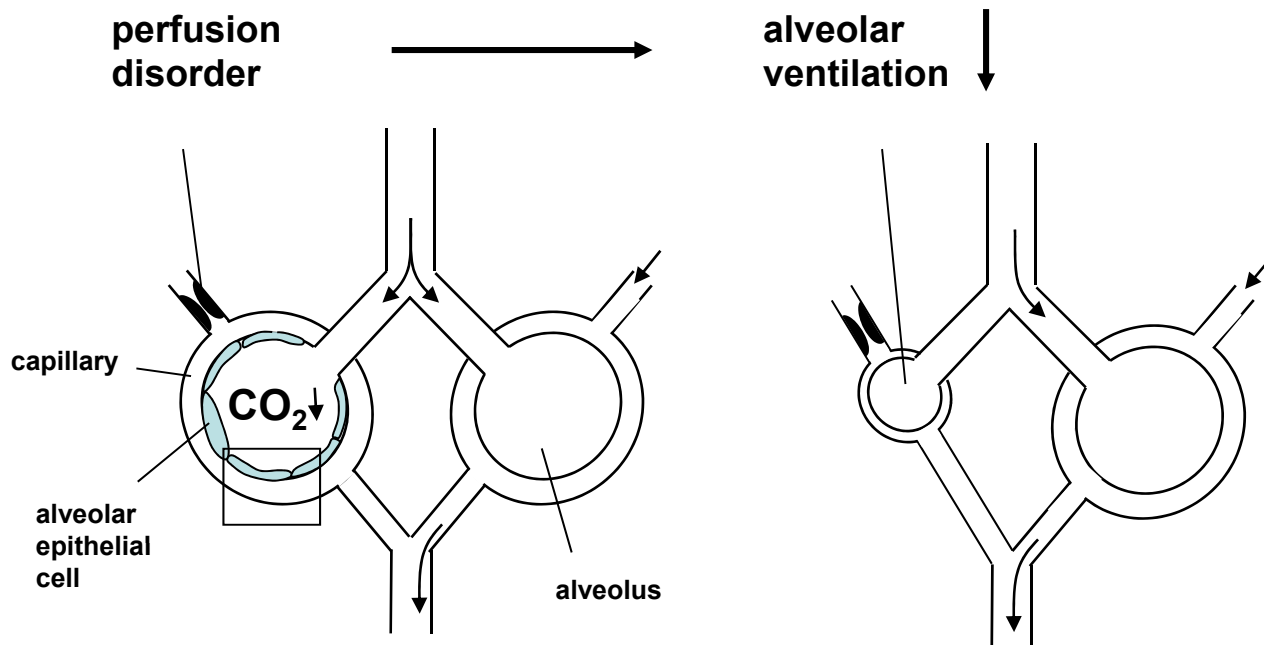


Figure 7

A



B

